A novel empirical method for predicting concentration polarisation in forward osmosis for single and multicomponent draw solutions

Ibrar Ibrar[a], Sudesh Yadav[a], Ali Altaee[a*], Alaa Hawari[b], Vinh Nguyen[a], John Zhou[a]

[a]*University of Technology Sydney, School of Civil and Environmental Engineering, Ultimo, NSW 2007, Australia.*

[b]*Department of Civil and Architectural Engineering, Qatar University, P.O. Box 2713, Doha, Qatar.*

**Corresponding author email address: ali.altaee@uts.edu.au*

Abstract

Concentration polarization is one of the inherent problems in forward osmosis membrane process. A quantitative evaluation of concentration polarization is therefore vital to understand its impact on the performance of the forward osmosis. Limited data in the literature exists for the diffusion coefficient of mixed electrolyte or multicomponent solutions, which makes the calculation of mass transfer coefficient and solute resistance to diffusion in forward osmosis complicated. Therefore, an empirical method based on a limited set of well-defined experiments for evaluating and predicting the concentration polarisation, water flux, and reverse solute flux is presented for single and mixed, or multi-ions draw solutions. The proposed method does not rely on the hydrodynamic conditions and flow regime in the system and provides an approach to measure and predict concentration polarisation, water flux, and reverse salt flux when the diffusion coefficient of a feed solution (FS) or draw solution (DS) is challenging to determine. The developed numerical method is two steps method to measure internal and external concentration polarisation using different concentrations of the draw and feed solutions. Experimental work was carried out with a single, and highly soluble sodium chloride (NaCl) DS and a mixture of NaCl and magnesium sulphate ($MgSO_4$) were used as a selected multicomponent DS. The results showed a 95% to 99% agreement with the experimental data.

Keywords: Forward Osmosis; Draw Solution; Concentration Polarisation; Reverse Salt Flux; Diffusion Coefficient.

1. Introduction

Forward osmosis (FO) has gained excellent popularity as a sustainable membrane separation process and a possible alternative to pressure-driven membrane processes [1-6]. While it has immense potential in wastewater treatment and seawater desalination, a major impediment in

its successful commercialization is the inherent problem of concentration polarization (CP) [2, 7-13]. Unlike pressure-driven membrane processes, the FO process experiences CP on both sides of the membrane [3, 11, 12, 14-22]. Although internal CP (ICP) plays a dominant role in flux decline in the FO process, external CP (ECP) effects cannot be overlooked when treating high salinity solutions, or when the FO membrane operates at a high water flux [23-25]. It is, therefore, vital to consider the impacts of both external and internal CP in the design and operation of the FO process [26-28].

The CP is measured in terms of its modulus. The two main parameters used in the FO process for measuring the moduli of external and internal CP are the mass transfer coefficient "*k*" and the solute resistance to diffusion "*K*". The most uncertain element in the theoretical determination of CP lies in the determination of the mass transfer coefficient "*k*" [29], which is usually estimated from a dimensionless correlation using an appropriate Sherwood relation for the flow regime. Numerous Sherwood relations have been proposed and extensively reviewed in the literature [12, 30-32]. Apart from the large number of different relationships that exist in the literature for mass transfer coefficient and Sherwood relations, most of these relations were developed for mass transfer either in smooth and non-porous systems or were derived from heat transfer-mass transfer analogies [33]. Whist FO membranes are semipermeable and often rough on a microscopic scale. The mass transfer also depends on fluid properties and rate of flow, and if these vary in the direction of flow, so does the mass transfer coefficient [34]. Some commercial suppliers of FO membrane modules, such as Porifera, provides limited information about the module (modules are sealed), which will further complicate the process of finding the mass transfer from Sherwood relations.

The solute resistivity (*K*), for example, is a function of the membrane characteristics (such as membrane porosity, tortuosity, and thickness), which are not readily available and requires an extensive procedure to determine [11]. Most importantly, the *K*, as well as the mass transfer "*k*" value, also depends on the value of the diffusion coefficient (D), which is easier to measure for a single salt solutions such as sodium chloride (NaCl), potassium chloride (KCl), and magnesium chloride ($MgCl_2$) [1, 11, 35]. However, there is limited data available in the literature for the diffusion coefficient of mixed electrolyte solutions except for NaCl and $MgCl_2$ [36]. The diffusion coefficient of mixed draw solution (DS) such as seawater or blended (two or more) DSs [37-39] that often used in the FO applications would be a mix of main diffusivities of individual draw solute and cross diffusivity of both the solution [40]. The co-existence of different species in a DS can also alter the diffusivity of a particular species [37]. For some DSs, the process becomes more complicated when dilution/suction parameters need to be considered [18]. In such instances, finding the value of *K* would be prone to errors. In addition, the asymmetry of the support structure also causes different diffusion behaviour depending

on the direction of flux and ion transport across the FO membrane [1]. Computer models based on computational fluid dynamics [24] and 2D finite element method (FEM) for predicting FO performance are complex and involve expertise in particular software. Several other new models have been developed recently by researchers including machine learning models [41], temperature/concentration parameter based solution diffusion models [23, 42], and spatial variation model [43]. So far, the current water flux models are exacting methodologies that require a lot of information about the FO membrane and flow characteristics of the filtration system.

Mixed or multicomponent DSs demonstrated excellent performance and widely used in the FO process [36, 38, 44, 45]. Although several models exist in the literature which addresses the CP for single solutes, the application of these models for quantifying CP in mixed DSs is questionable as well as non-existent in the literature. The objective of this study is two-fold. Firstly, to develop an empirical method to measure CP profiles in the FO process in both membrane orientations for single and mixed DS. Secondly, the proposed method was validated to predict dilutive and concentrative CP, water flux and reverse salt flux in the FO process for single and mixed DS. The method used in this study does not require information about the flow regime in the FO process and special membrane characteristics (such as structure parameter) to calculate water flux and reverse salt flux, and hence, can also be extended to ternary and quaternary mixtures in osmotically-driven membrane processes.

2. Theory and Model

2.1. Modelling dilutive concentration polarization (CP)

Concentration polarization (CP) in the FO process occurs on both sides of the FO membrane, i.e., the draw and feed sides. Dilutive concentration polarization due to concentration dilution occurs on the DS side, while concentrative concentration polarization occurs on the feed solution side. Dilutive and concentrative CP is taking place simultaneously, making the process of predicting the moduli of concentrative and dilutive concentration polarization in the FO process more complicated. The modulus of concentrative CP, however, will be negligible when the feed solution is de-ionized (DI) water. Hence, the modulus of dilutive CP can be separately measured, as presented in **Fig.** A.1a (Appendix A.1) for AL-DS mode (when the active layer faces the draw solution) and **Fig.** A.1b (Appendix A.1) for AL-FS mode (when the active layer faces the feed solution).

According to the modified solution-diffusion model based on film theory, water flux across the FO membrane is given Eq**.** [1].

$$J_w = A_w\,[(\pi_{Db} - \pi_{Fb}) - \Delta P] \qquad [1]$$

where $\boldsymbol{A_w}$ is the pure water permeability coefficient of the FO membrane, $\boldsymbol{\pi_{Db}}$ and $\boldsymbol{\pi_{Fb}}$ are bulk osmotic pressures of the DS and FS (feed solution), respectively, and $\Delta\boldsymbol{P}$ is the transmembrane hydraulic pressure. Eq. [1] calculates the water flux as a function of driving force only based on the concentration difference and is valid only in the absence of CP phenomena. In practice, the flux through an asymmetric FO membrane is far lower than predicted by Eq. [1].

Most commercial FO membranes have a rejection rate of over 90% to ions. It is assumed in this study that the FO membrane is completely selective (complete ion rejection and a reflection coefficient of 1). When the FS is a DI water, the osmotic pressure of the feed side will be insignificant, and hence the effect of CP on the feed side is negligible. However, the impact of dilutive CP on the DS side still exists due to the dilution of DS by permeate flow (dilutive external CP) in the AL-DS mode and inside the support layer (SL) in the AL-FS (dilutive internal CP). As such, Eq. [1] can be expressed in terms of dilutive CP at the draw solution side ($\boldsymbol{CP_D}$).

$$J_w = A_w(CP_D\pi_{Db}) - \Delta P] \qquad [2]$$

where $\boldsymbol{CP_D}$ is the dilutive external CP correction factor on the DS side. The osmotic pressure at the membrane surface π_{DM} after correction for the dilution factor can be expressed by Eq. [3].

$$\pi_{DM} = \pi_{Db}CP_D \qquad [3]$$

Substituting Eq. [3] in Eq. [2] yields,

$$J_w = A_w\,(\pi_{DM} - \Delta P) \qquad [4]$$

$$\pi_{DM} = \frac{J_w}{A_w} + \Delta P \qquad [5]$$

Since the FO process is driven by the osmotic pressure gradients across the membrane, the hydraulic pressure in Eq. [5] is equal to zero, $\Delta\boldsymbol{P}$ **=0**. From Eq. [5] the osmotic pressure difference π_{DM} across the AL can be calculated using experimental water flux and pure water permeability coefficient $\boldsymbol{A_w}$ [46]. Rearranging Eq. [3], the modulus of dilutive CP at the DS membrane interface is given by Eq. [6].

$$CP_D = \frac{\pi_{DM}}{\pi_{Db}} \quad [6]$$

Experimentally, π_{Db} is calculated as the average osmotic pressure of the inlet and outlet DS, whereas, experimental water flux in the FO process $\boldsymbol{J_{we}}$ is given by Eq. [7]:

$$J_{we} = \frac{(W_t - W_i)}{1000 * A * t} \quad [7]$$

where A is the membrane area, t is the filtration time, and W_t and W_i are weights of permeate at t time and initial time, respectively. In the FO process, the value of $\boldsymbol{CP_D}$ is less than unity due to dilution of the DS, while $\boldsymbol{CP_D}$ value equals unity refers to zero dilutive CP. For a given FO membrane with a known $\boldsymbol{A_w}$ and DI water FS, experimental water flux can be calculated from Eq. [7] then compensated in Eq. [5] to calculate π_{DM}. $\boldsymbol{CP_D}$ can be obtained from Eq. [6]; this process will be repeated for a range of DS concentrations (single or mixed DS) using a DI water FS. **Fig.** 1a shows the relationship between J_{we} and $\boldsymbol{CP_D}$ for several DS concentrations (curves are a replication of experimental data). Practically, the $\boldsymbol{CP_D}$ of any DS within the range of concentrations used in **Fig.** 1a can be predicted by knowing water flux (DI water feed or saline feed) in the FO process. **Fig.** 1b presents the relationship between the theoretical osmotic pressure π_{Db} and the effective osmotic pressure (π_{DM}) in the FO process for DI water FS. From Fig 1a and 1b, theoretical water flux in the FO process with DI water feed can be predicted by knowing the bulk osmotic pressure of the DS. From Fig 1b, the calculated π_{Db} will be used to predict π_{DM} using regression analysis in the FO process, then theoretical water flux $\boldsymbol{J_{wt}}$ for DI water feed and different DS concentrations can be estimated using Eq. [4].

In general, the modulus of dilutive CP, $\boldsymbol{CP_D}$, of any DS within the range of concentrations in **Fig.** 1a can be predicted by knowing the experimental water flux in the FO process. Furthermore, water flux and $\boldsymbol{CP_D}$ in the FO process with DI water feed solution can be theoretically predicted using the relationship between the bulk osmotic pressure $\boldsymbol{\pi_{Db}}$ and $\boldsymbol{\pi_{DM}}$ in **Fig.** 1b, then compensating in Eq. [4] to calculate J_w or Eq. [6] to calculate $\boldsymbol{CP_D}$.

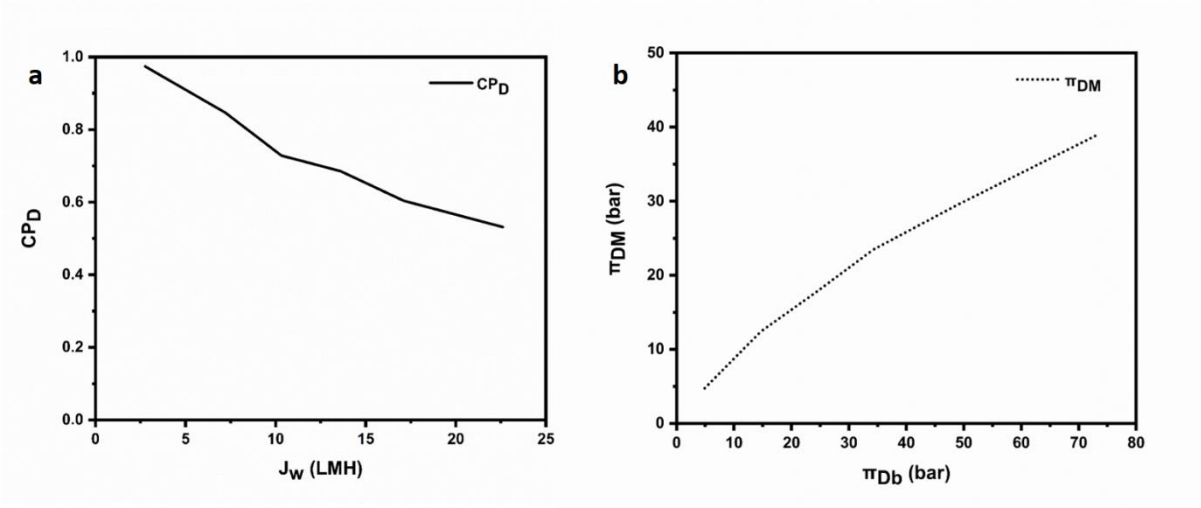

Figure.1. Water flux in the FO experiment using DI water FS and NaCl DS. **a)** Experimental water flux vs. the modulus of $\boldsymbol{CP_D}$. **b)** A plot of bulk osmotic pressure π_{Db} against the osmotic pressure at the membrane surface on the DS side π_{DM}. The concentration of DS ranges from 0.1M to 1.5M at 20°C.

2.2. Modelling concentrative concentration polarization (CP)

Concentrative and dilutive CP co-occur on the feed and draw sides of the FO membrane. The effect of concentrative CP can be ignored when DI water is the FS but becomes significant as the salinity of FS increases. Two types of FO experiments are required to find out the effects of concentrative and dilutive CP in the FO process. In the first set of experiments, DI water will be the FS [**Fig.2**] to calculate a correlation between J_{we} and $\boldsymbol{CP_D}$, as illustrated in section 2.1. In the second set of experiments, the FO process will be performed with different FS and DS salinities to estimate the value of $\boldsymbol{CP_F}$. Eq. [1] calculates water flux in the FO process, using DI water FS. However, Eq. [1] overestimates water flux in the FO process by 50% [47]. Practically, freshwater transport across the FO membrane dilutes the DS ($\boldsymbol{CP_D}$ on the draw side) and concentrating the FS resulting in a concentrative CP on the feed side ($\boldsymbol{CP_F}$ on the feed side). Experimentally, water flux in the FO process using two solutions of different concentrations is given by the following Eq.:

$$J_w = A_w(\pi_{DM} - \pi_{FM} - \Delta P) \qquad [8a]$$

$$\Delta\pi = \frac{J_w}{A_w} + \Delta P \qquad [8b]$$

where, π_{FM} is the osmotic pressure of the FS at the membrane surface, and $\Delta\pi$ is the net osmotic pressure driving force. In Eq. [8], $\Delta\boldsymbol{P}$ can be cancelled since the hydraulic pressure

gradient is equal to zero in the FO process. Eq. [8a] can be expressed in terms of the moduli of dilutive and concentrative CP for the draw and FS, respectively, as the following:

$$J_w = A_w(CP_D\pi_{Db} - CP_F\pi_{Fb}) \qquad [9]$$

where, $\boldsymbol{CP_F}$ represents the modulus of concentrative CP. In Eq. [9], π_{Db} and π_{Fb} are the bulk osmotic pressure of DS and FS, and J_w can be experimentally calculated from Eq. [7]. Once $\boldsymbol{J_{we}}$ is experimentally determined, the modulus of dilutive CP $\boldsymbol{CP_D}$ can be predicted from Fig. 1a from a correlation between experimental water flux $\boldsymbol{J_{we}}$ and the amount of dilution caused by permeating water ($\boldsymbol{CP_D}$). Substituting J_{we}, $\boldsymbol{CP_D}$, π_{Db} and π_{Fb} in Eq. [9] to calculate the modulus of concentrative CP, $\boldsymbol{CP_F}$. Then, the bulk osmotic pressure π_{Fb} will be plotted against the osmotic pressure at the membrane surface (π_{FM}) in Fig. 2a and J_{we} will be plotted as a function of π_{FM} in **Fig.** 2b. Thus, the theoretical value of water flux in the presence of FS can be predicted based on values of π_{FM} in Fig.2b. Mathematically, $\boldsymbol{CP_F}$ is described as the ratio of π_{FM} to π_{Fb} as given by Eq.[10].

$$CP_F = \frac{\pi_{FM}}{\pi_{Fb}} \qquad [10]$$

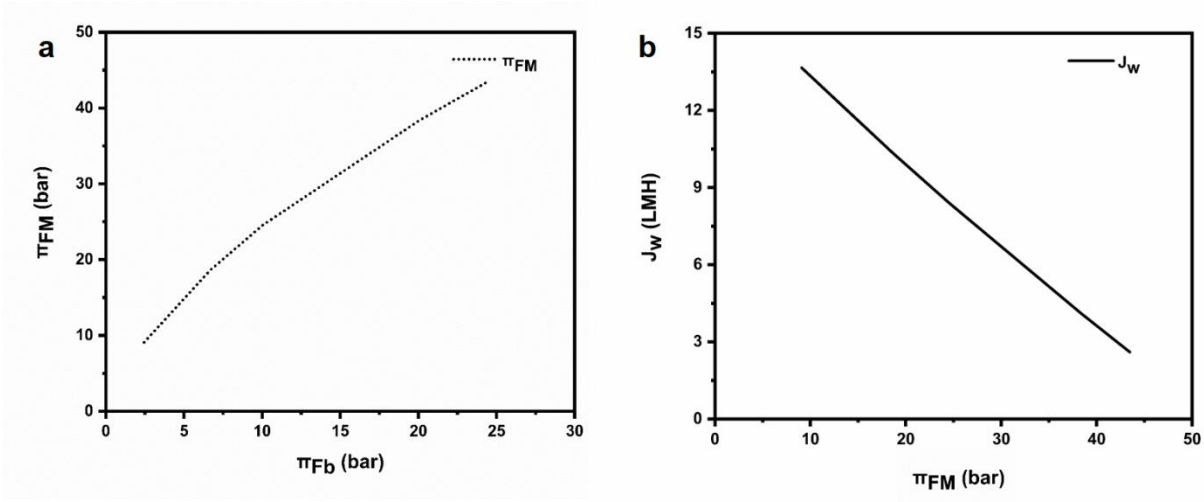

Figure.2. Water flux in the FO experiment using NaCl FS and DS. **a)** A plot of osmotic pressure at the membrane surface π_{FM} and bulk FS osmotic pressure π_{Fb}. **b)** Experimental water flux vs π_{FM}. The concentration of DS is 1M at 20°C, and the concentration of FS ranges from 0.05 to 0.5M at 20°C.

In the FO process, along with the water flux, there is also a reverse salt flux (RSF) from the DS to the FS. Ideal FO membrane has a complete rejection of solutes, but in practice, a small

amount of the draw solute would transport across the membrane. Mathematically, the salt flux from DS to the FS can be estimated by Eq. [11].

$$J_{st} = B(C_{DM} - C_{FM}) \quad [11]$$

In Eq. [11] J_{st} is the theoretical RSF, C_{DM} is the concentration of DS at the membrane surface on the DS side, and C_{FM} is the concentration of FS at the membrane surface on the feed side. When DI water is the FS, and all salt in feed is from RSF, Eq. [11] can be modified as:

$$J_{st} = B\left(\frac{\pi_{DM}}{nRT}\right) \quad [12]$$

Once the osmotic pressure at the membrane surface is determined using Eq. [5], the theoretical RSF can be calculated using Eq. [12] with DI water FS and Eq. [11] for NaCl FS. For model verification, the experimental RSF was calculated using Eq. [13].

$$J_{se} = \frac{V_f\, C_f - V_i C_i}{A*t} \quad [13]$$

where $\boldsymbol{V_f}$ and $\boldsymbol{C_f}$ is the final volume and concentration of the FS, respectively, and $\boldsymbol{V_i}$ and $\boldsymbol{C_i}$ is the initial volume and concentration of the FS at the start of the FO experiment. ***A*** represents the total membrane area, and ***t*** is the filtration time of the FO run.

In practice, for a given FO membrane, the water permeability coefficient will be experimentally obtained. Then, two steps experimental work will be carried out to calculate $\boldsymbol{CP_D}$ and $\boldsymbol{CP_F}$ in the FO membrane. The first set of experiments uses DI water FS and saline DS of different concentrations to calculate $\boldsymbol{CP_D}$ in the FO process using the procedure explained in section 2.1. The impact of concentrative CP and dilutive CP will be obtained in the second set of experiments, which uses a range of feed and draw concentrations to calculate $\boldsymbol{CP_F}$ in the FO process, as illustrated in section 2.2. To predict water flux in the FO process for a known feed and draw concentrations (within the studied concentrations), π_{FM} will be estimated from Fig. 2a using the corresponding values of π_{Fb} to obtain $\boldsymbol{CP_F}$. Finally, water flux will be estimated from Fig. 2b. The reverse salt flux can be obtained using Eq. [12] with DI water feed and Eq. [11] for a saline FS. A schematic diagram of water flux and CP measurements in the FO process is illustrated in **Fig. 3.** It should be noted that water flux and reverse salt flux in this method will be directly affected by the testing conditions of the FO process such as feeds flow rate, the temperature of feed and draw solution, the concentration of feed and draw solution.

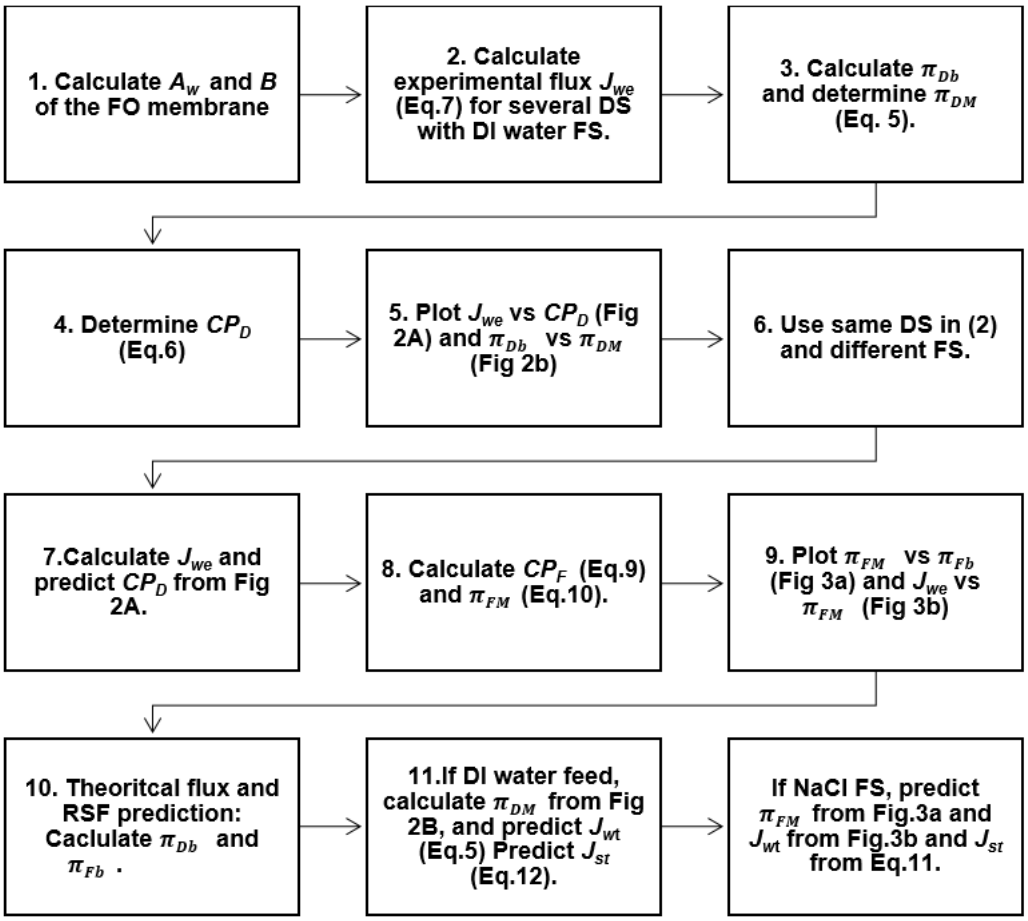

Figure. 3. Schematic diagram of calculation and prediction of the CP in the FO process.

3. Materials and Methods

3.1. Forward osmosis cross-flow system and membrane

A schematic diagram of the laboratory-scale unit is shown in **Fig. 4**. The FO cell (CF042D) used in this study was obtained from Sterlitech Corporation (USA) and featured an active membrane area of 42 cm^2 (0.0042 m^2). Two Cole-Parmer Micro-pumps with Console Drive, PEEK (Sterlitech-USA) were used for FS and DS pumping. A panel mount flow meter F-550 (Sterlitech –USA) was used to measure the volumetric flow rate of the FS and the DS. The flow rate was fixed at 2 litres per minute (cross-flow velocity of 36 cm/s) for both the feed and the draw side, and the cell was operated in co-current cross-flow. A digital balance (EK-15KL) connected to a computer was used on the draw side to record the increase in the weight of the DS. Water flux was calculated from the weight change of the DS. The experiment was

operated at an ambient lab temperature of 21 ±1.5 ^{0}C. Immersion circulators (Sterlitech-USA) were used to maintain the temperature of feed and DS when required. A conductivity meter (Hach HQ14d) on both draw and feed side was used to record the change in conductivity of the draw and FS.

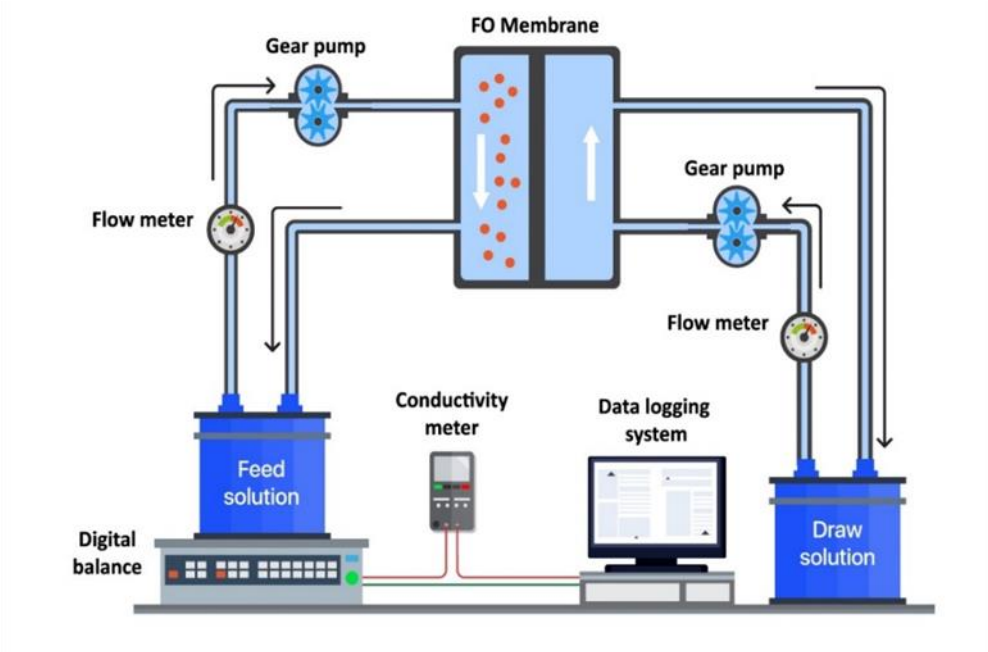

Figure.4. Diagram of the lab-scale forward osmosis system. Co-current cross-flow of the feed and DS was used in all the experiments.

This study used a flat sheet cellulose triacetate (CTA) FO membrane "FTSH2O" provided by Sterlitech Corporation and manufactured by Fluid Technology Solutions. The membrane was soaked overnight in DI water to ensure complete wettability. At the beginning of each run, it was flushed with DI water to remove any additives.

3.2 Feed and draw solutions

All chemicals used in experiments were analytical grade obtained from Sigma Aldrich, Australia. NaCl DS was prepared by dissolving an analytical grade NaCl in DI water. Mixed DS was prepared by mixing NaCl solution with $MgSO_4$ (magnesium sulphate, molecular weight 120.37 g/mol). NaCl was used as a major solute and $MgSO_4$ as a minor solute (0.1M) in the solution. The FS used in this study, depending on the objective of experiments, was either DI water or NaCl solution with concentration ranging 0.05M to 0.5M. The osmotic pressure of all solutions was calculated by the Van't Hoff Eq.:

$$\pi = iCRT \qquad [14]$$

where *i*= number of ions produced during dissociation of solute, *R* is the universal gas constant (0.0820 L atm $mol^{-1}K^{-1}$), *C* is the molar concentration of the solute (mole/L), and *T* is the absolute temperature (kelvin).

3.3. Experimental protocol

Two types of experiments were carried out to measure the effects of CP in the FO process in both the AL-DS and the AL-FS orientation. The first set of experiments used DI water FS, and single salt NaCl DS with concentrations between 0.1M and 1.5M to measure the dilutive CP ($\boldsymbol{CP_D}$) on the DS side. In the second set of experiments, DI water FS was replaced with NaCl FS to measure the effects of concentrative CP ($\boldsymbol{CP_F}$). The concentration of FS was from 0.05M to 0.5M NaCl. After each run, the membrane was rinsed with DI water at a 2.8 LPM flow rate (cross-flow velocity of 51 cm/s) for at least 30 minutes to remove any salts accumulated from a previous test. A similar protocol was used for mixed salt experiments, except that a constant 0.1M $MgSO_4$ was added to the corresponding NaCl DS. Each experiment was conducted at least 2 times, and the average results were reported in this study.

4. Results and Discussions

4.1. Membrane intrinsic properties

The pure water permeability $\boldsymbol{A_w}$ and salt permeability $\boldsymbol{B}$ was determined through a cross-flow RO (reverse osmosis) setup. The detailed procedure is listed in Appendix A.1. Primarily, we need the value of $\boldsymbol{A_w}$ and $\boldsymbol{B}$ for modelling in this study. The $\boldsymbol{A_w}$ value used in the calculation in this study was 0.58 $Lm^{-2}h^{-1}bar^{-1}$. The membrane $\boldsymbol{B}$ value used in the prediction of RSF was 0.32±0.05 $Lm^{-2}h^{-1}$. These values are comparable to previously reported for this membrane [35].

4.2. Quantification of CP for mixed DS

CP is usually measured in terms of its modulus. The dilutive concentration polarization modulus is defined as the ratio of the osmotic pressure of the DS at the membrane surface to the bulk osmotic pressure of DS [Eq. 6]. According to the previous mass transfer models in the literature [12], dilutive CP modulus is usually less than 1, and concentrative CP modulus is greater than 1. To measure the effect of $\boldsymbol{CP_D}$ and $\boldsymbol{CP_F}$, NaCl was used as a DS, and FS was DI water in the first set of experiments. In the next set of experiments, FS was replaced with 0.05M to 0.5M NaCl solution to calculate the values of $\boldsymbol{CP_F}$.

4.2.1. AL-DS mode: Quantification of CP_D NaCl DS-DI water FS

In the AL-DS mode, experimental water flux, J_{we} and experimental RSF J_{se} curves (calculated with different DS concentrations from Eq. [7] and Eq. [13]) are presented in Fig. 5a as a function of the net osmotic driving force. Water flux is presented on the primary y-axis, whereas RSF is presented on the secondary y-axis. The concentrations of DS were 0.1, 0.3M, 0.5M, 0.7M, 1M, and 1.5M NaCl, while DI water was the FS to minimize the effect of concentrative CP, i.e., $\boldsymbol{CP_F \approx 0}$. As the DS concentration increased gradually from 0.1 to 1.5M, water flux in the FO process increased. The concentration of NaCl in the FS due to reverse salt flux (RSF) was measured at the end of the FO experiments and found to be very low (<100 mg/L) to have a significant effect on the osmotic pressure of the FS. The osmotic pressure at the membrane AL surface π_{DM} was obtained from Eq. [5], and is presented in Fig. 5b as a function of the osmotic pressure of bulk draw solution. The value of π_{DM} represents the actual osmotic pressure at the membrane surface responsible for the water transport across the FO membrane. The osmotic pressure π_{DM} was divided by the osmotic pressure of the bulk draw solution to obtain the $\boldsymbol{CP_D}$ modulus using Eq. [6]. The values of $\boldsymbol{CP_D}$ were calculated for each DS concentration and are presented as a function of the experimental permeate flux in Fig. 5c and as a function of NaCl draw solution concentration in Fig. 5d.

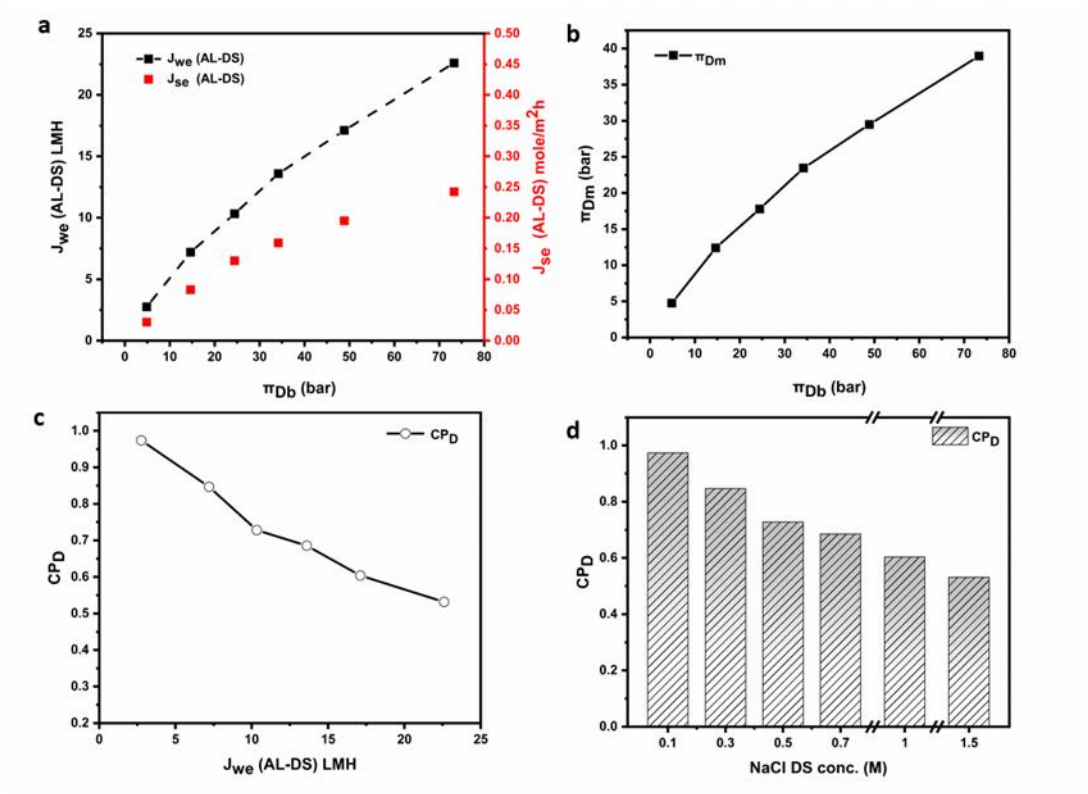

338

339 **Figure 5**. Quantifying dilutive concentration polarisation in the FO process for AL-DS mode
340 with DI water feed solution and NaCl DS (0.1-1.5M) (a) Plot of experimental water flux J_{we} and
341 experimental RSF J_{se} against the bulk osmotic pressure π_{Db}, (b) Plot of osmotic pressure at
342 the membrane surface π_{DM} against bulk DS osmotic pressure π_{Db} (c) A plot of dilutive CP
343 modulus $\boldsymbol{CP_D}$ as a function of experimental water flux J_{we} (d) A plot of dilutive CP modulus
344 $\boldsymbol{CP_D}$ as a function of NaCl DS concentration.

345

346 Results in Fig. 5c and Fig.5d show that the $\boldsymbol{CP_D}$ became severer (farther from unity) with
347 increasing the concentration of DS and increased water flux. In other words, the value of $\boldsymbol{CP_D}$
348 is strongly dependent on water flux [1]. Higher DS concentrations result in higher permeation
349 flux, and hence creating a higher degree of dilution of the DS on the surface of the AL. For
350 example, the most severe $\boldsymbol{CP_D}$ was 0.52 for 1.5M NaCl DS, indicating that the osmotic
351 pressure of DS at the membrane surface is almost half of that in bulk DS. At higher water flux,
352 therefore, the effects of dilutive external CP can become a limiting factor in the FO process [2,
353 48]. At very low water fluxes and DS concentration such as 0.1M, the effects of $\boldsymbol{CP_D}$ is almost
354 negligible ($\pi_{DM} \approx \pi_{Db}$).

355

356 **4.2.2. AL-DS mode: Quantification of CP_F NaCl DS-NaCl FS**

357

When the feed solution in the FO process is a DI water, the osmotic pressure at the FS side of the membrane will be negligible, and the relationship between J_{we} and $\boldsymbol{CP_D}$ is illustrated in Fig. 5c. For the FO process with a saline FS, additional information should be available to calculate the $\boldsymbol{CP_F}$ in the FO process. NaCl solution of concentration between 0.05 and 0.5M was the FS in the FO process to measure the concentrative CP, $\boldsymbol{CP_F}$, in the FO membrane at 1M NaCl. The FO process was performed in the AL-DS mode to study the moduli of $\boldsymbol{C_{PF}}$ and the $\boldsymbol{C_{PD}}$. The two CPs are acting simultaneously on the FO membrane leading to a reduction in the experimental permeate flux J_{we} (Fig. 6a). As shown in Fig.6a, water flux increased with increasing the net osmotic pressure $\Delta\pi$. The modulus of $\boldsymbol{C_{PD}}$ can be obtained from the correlation between J_{we} and $\boldsymbol{C_{PD}}$ from Fig. 5c, which shows water flux at different osmotic pressure gradients. In effect, the dilutive CP is mainly caused by water flux permeating across the membrane, diluting the concentration of the DS at the boundary layer. Compensating in Eq. [9] to obtain the modulus of $\boldsymbol{C_{PF}}$ at different water flux, and results are shown in Fig. 6b. The moduli of $\boldsymbol{CP_D}$ and $\boldsymbol{CP_F}$ are presented in Table A.1.3 (Appendix A.1). As the concentration of FS increases, water flux and the modulus of $\boldsymbol{CP_D}$ decreases. In other words, as $J_{we} \rightarrow 0$ the modulus of $\boldsymbol{CP_D}$ is approaching 1 [37].

At low FS concentration, $\boldsymbol{CP_D}$ will be more substantial while the role of $\boldsymbol{CP_F}$ will be insignificant [49] and this explains the levelling of the modulus of $\boldsymbol{CP_F}$ at lower FS concentration (Fig. 6b). The modulus of $\boldsymbol{CP_F}$ increases at an exponential rate as the water flux increases and vice versa. Once the value of $\boldsymbol{CP_F}$ is available, the value of π_{FM} can be found from Eq. [10]. The correlation between π_{FM} and π_{Fb} is presented in Fig. 6c and experimental water flux (J_{we}) and π_{FM} is presented in Fig. 6d. The modulus of $\boldsymbol{CP_F}$ at any point can also be obtained from the slope of the line in Fig. 6c between π_{FM} and π_{Fb} . As the concentration of FS increases, the osmotic pressure at the membrane surface also increases (Fig. 6c), leading to a reduction in the osmotic driving force due to the severe $\boldsymbol{CP_F}$.

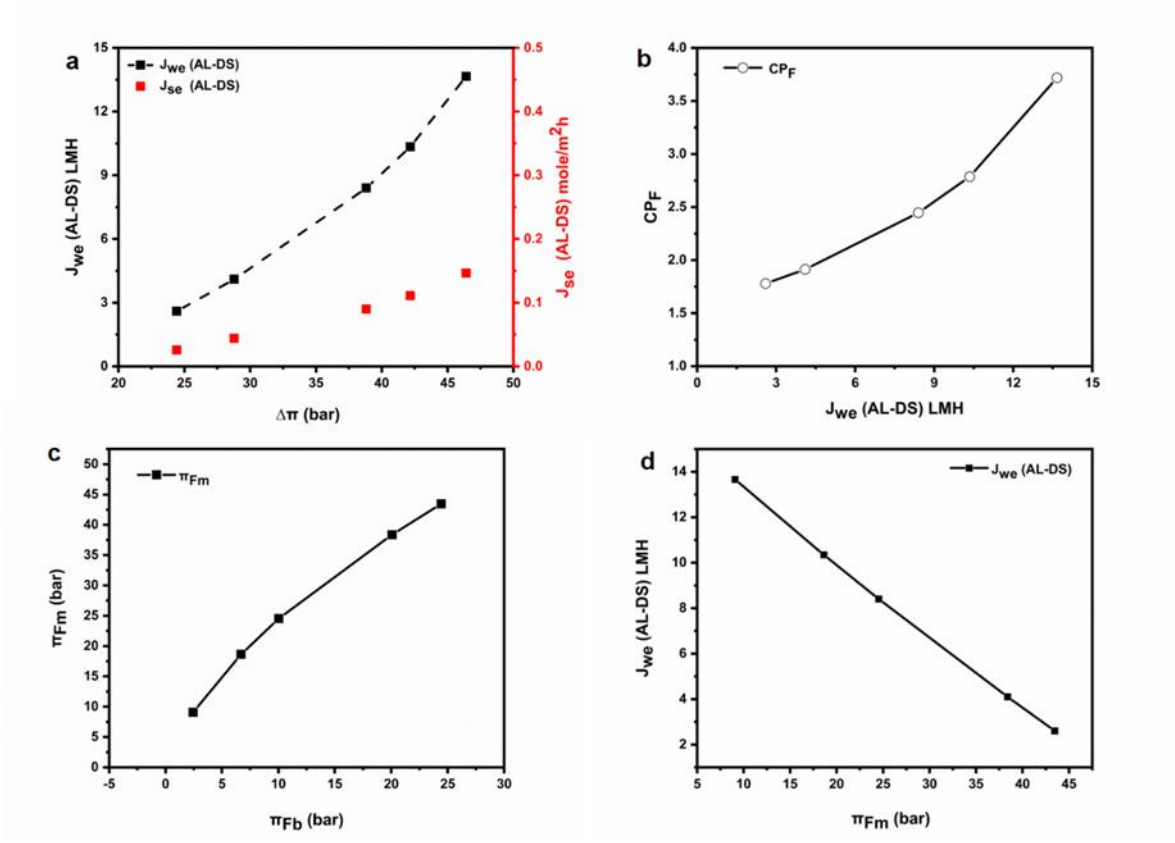

383

384 **Figure 6**. Quantifying concentrative concentration polarisation in the FO process for AL-DS
385 mode with NaCl feed solution (0.05 to 0.5M) and NaCl DS (1M), (a) Plot of experimental water
386 flux J_{we} and experimental RSF J_{se} against the bulk osmotic pressure (b) Plot of concentrative
387 CP modulus $\boldsymbol{CP_F}$ against experimental water flux J_{we} (c) Plot of osmotic pressure at the
388 membrane surface on the feed side π_{FM} as a function of π_{Fb} (d). A plot of experimental water
389 flux J_{we} as a function of osmotic pressure at the membrane surface on the feed side π_{FM} .

390

391 The correlations in Fig. 6c and Fig.6d can also be employed to predict theoretical water flux
392 for different feed solution concentrations, once the theoretical value of π_{FM} is available. These
393 relations will be used to predict the theoretical water flux in the FO process for different feed
394 solution concentrations using regression analysis.

395

396 **4.2.3. AL-FS mode: Quantification of CP_D NaCl DS-DI water FS**

397

398 When the FO membrane is operated in the AL-FS orientation, $\boldsymbol{CP_D}$ occurs inside the SL while
399 $\boldsymbol{CP_F}$ is on the AL side. In the case of DI water FS, the $\boldsymbol{CP_F}$ values are insignificant due to the
400 negligible osmotic pressure on the FS side (π_{Fb}=0.08 bar for 100ppm NaCl). Water permeates
401 inside the SL and dilutes the DS, leading to a dilutive CP inside the SL. Initial tests were
402 performed with DS concentrations ranging from 0.1M to 1.5M, and the water flux and RSF

curves as a function of the osmotic driving force are presented in **Fig.** 7a. Water flux in the AL-FS mode is less than that in the AL-DS mode for the same driving force due to the severe ***CP$_D$***, which exists inside the SL. As the boundary layer exists now inside the SL, it is difficult to mitigate it using a cross-flow velocity of 36 cm.sec^{-1} in our study. The RSF in the AL-FS mode was also lowered compared to the AL-DS mode. The numerical value of π_{DM} was calculated according to Eq. [5] and is presented as a function of the DS osmotic pressure (Fig. 7b). ***CP$_D$*** was calculated from Eq. [6] and plotted against the experimental water flux in Fig. 7c and the concentration of the DS in Fig. 7d.

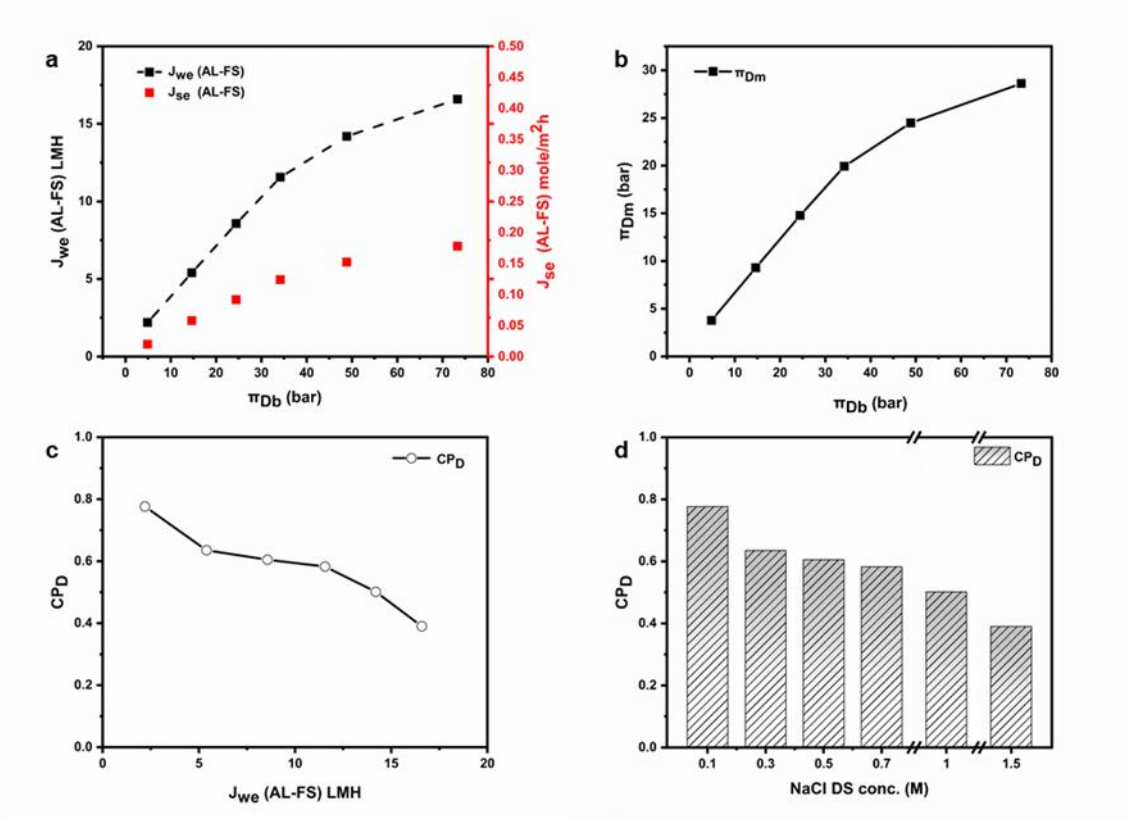

Figure 7. Performance of FO membrane in the AL-FS mode with single salt DS, (7a) Water flux and RSF in the FO mode with single salt NaCl solution as a function of the osmotic driving force,(7b) Plot of osmotic pressure at the membrane surface π_{DM} as a function of bulk NaCl DS osmotic pressure π_{Db} (7c) Plot of dilutive CP ***CP$_D$*** against the experimental water flux, (7d) Dilutive CP ***CP$_D$*** as a function of NaCl DS concentration.

As the concentration of DS is increased, ***CP$_D$*** tends to farther away from the value of 1, depicting its severity. However, from 0.3M to 1M, an increase in DS concentration and water flux decreases the modulus by a tiny percentage (**Fig.** 7b and **Fig.** 7c a flatter curve for the modulus). This phenomenon also is known as the ICP self-compensation effect [19] means that an increase in ICP or CPD compromises any increase in DS concentration or driving force. Above 1M, the increase in the ICP becomes more severe, as marked by a greater

increase in the modulus of CP_D for 1.5M DS. This severity makes the experimental water flux highly non-linear at high DS, as depicted in Fig.7a.

4.2.4. AL-FS mode: Quantification of CP_F NaCl DS-NaCl FS

In order to measure the concentrative CP modulus, CP_F, FS was replaced with 0.05 to 0.5M NaCl, and the concentration of DS was 1M NaCl. The experimental permeate flux J_{we} and experimental RSF J_{se} as a function of osmotic driving force are presented in Fig. 8a. Both the water flux and RSF were lowered in the AL-FS orientation compared to the AL-DS. The CP_D was predicted from Fig. 7c and the CP_F was calculated from Eq. [9], the results of CP_D and CP_F are listed in Table A.1.4 (Appendix A.1). The CP_F as a function of experimental water flux is presented in Fig. 8b. Compared to the AL-DS mode, severe dilutive CP resulted in a smaller water flux when the membrane was operating in the AL-FS mode. Once CP_F is determined the value of π_{FM} can be found using Eq.[10]. Fig. 8c presents the correlation between π_{FM} and π_{Fb}. For any concentration of FS (within the range of 0.05 to 0.5M) and 1M DS, the value of π_{FM} can be estimated from **Fig.** 8c. Finally, **Fig.** 8d can be used for the prediction of theoretical water flux with any FS concentration from 0.05M NaCl to 0.50M NaCl and 1M DS.

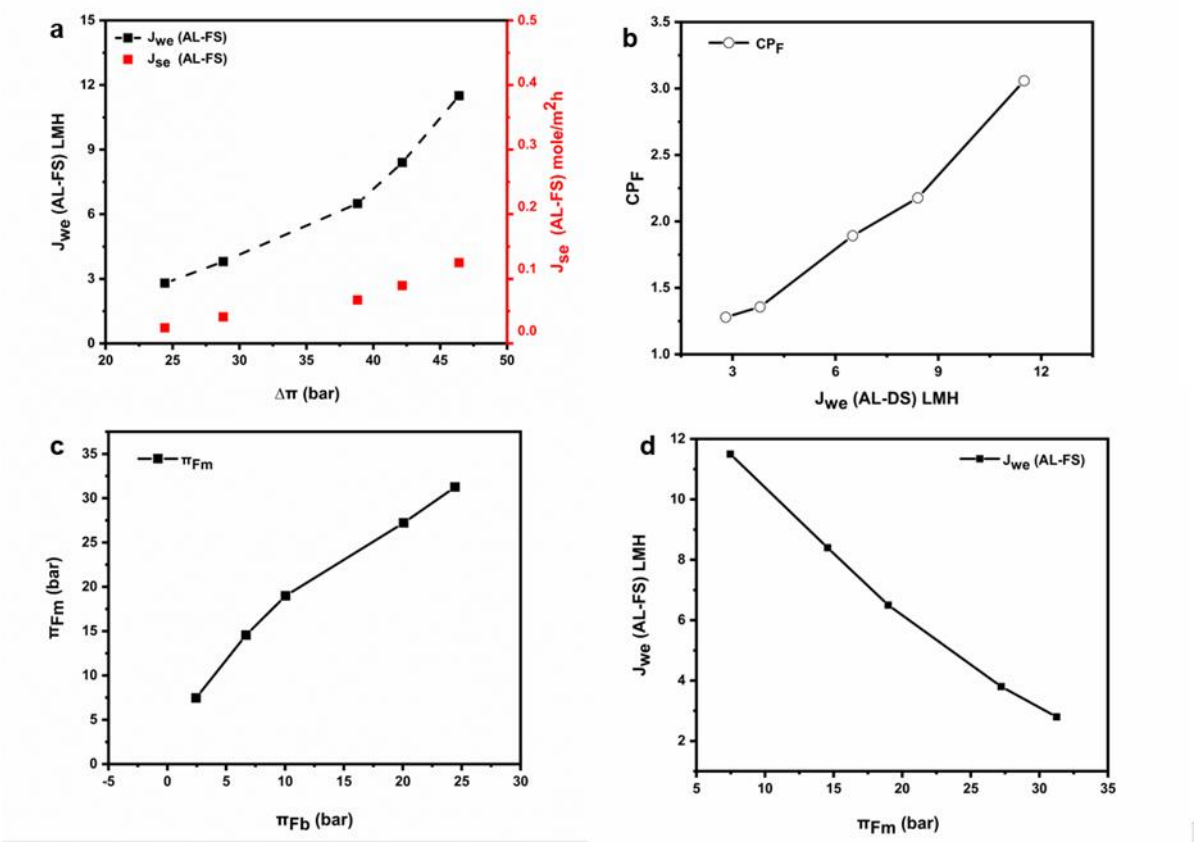

Figure 8. Performance of FO membrane in AL-FS mode with 1M NaCl DS and 0.05M to 0.5M NaCl FS, (a) Plot of experimental water flux and RSF against bulk osmotic pressure, (b) Plot of concentrative CP CP_F against experimental water flux (c) Plot of bulk FS osmotic pressure

π_{Fb} against osmotic pressure at the membrane surface π_{FM}. d. Correlation between experimental water flux and osmotic pressure at the membrane surface π_{FM}.

4.3. Quantification of CP for mixture DS

The osmotic pressure of a solution is affected by adding a second solute to the solution [45]. The addition of multivalent ions to a solution also affects the structure of the solvent [50]. It has been demonstrated that water structure is ordered by small or multivalent ions and disordered by large or monovalent ions [50]. On the one hand, multivalent ions such as Mg^{2+} and SO_4^{-2} will tend to order the solvent structure. On the other hand, large monovalent ions such as Na^+ will try to disorder the water structure in mixed draw solution experiments. The ions effect on the water can also be explained by a competition between ion-water interactions [51]. Small ions of high charge density bind to water molecules strongly, whereas, there is weak binding between large monovalent ions and water molecules relative to the strength of water-water interaction in the bulk solution [51]. Thus, different CP behaviour is expected for mixed solutions. To investigate the CP moduli in mixed DS, a 0.1M $MgSO_4$ was added to the corresponding NaCl DS of concentrations ranging from 0.1M to 1.5M. The CPs were investigated in both the AL-DS and the AL-FS mode using DI water and NaCl salt ranging from 0.05 to 0.5M as a FS. The experimental protocol was exactly the same as section 4.2.

4.3.1. AL-DS mode: Quantification of CP_D mixture DS-DI water FS

Fig. 9a shows the experimental water flux J_{we}, and RSF J_{se} as a function of the osmotic driving force for DI water FS and NaCl solution (0.1 to 1.5M) + 0.1$MgSO_4$ DS. The osmotic driving force increased slightly with the increase of the concentration of mixture DS, yet the average water flux for the DS was slightly less than that for NaCl DS only. The slight decrease in the water flux for a mixture DS can be attributed to the swelling of the cellulose acetate polymer in the presence of divalent magnesium cation [52]. The presence of $MgSO_4$ in the DS might cause swelling of the AL, making it slightly less permeable to water molecules [53]. Compared to a single NaCl DS, RSF decreased in the FO process with a mixture DS. Similar results with a mixed DS for reducing the RSF has been reported in previous studies [36]. The decrease in the RSF can be simply attributed to the larger molecular size of the $MgSO_4$ and the smaller diffusivities of the Mg^{2+} and SO_4^{-2} ions. The co-existence of mixed solutions also affect the

diffusivity of the species in the mixed draw solutions mainly because of the main diffusivities (flux of a component with its concentration gradient) and cross diffusivities (flux of a component with the gradients of all other components in the mixed DS) that arise from mixing the two solutions. The net value of a diffusion coefficient in a multicomponent DS will be the result of interaction between all species in that solution. For binary mixtures such as NaCl+$MgSO_4$, there is limited data available from the literature for the mutual diffusion coefficient value. Even if such data is available in the literature, they are valid only for the experimental conditions for that particular experiment or study and invalid outside the experimental conditions. The dilutive effects of $\boldsymbol{CP_D}$ in the AL-DS mode leads to a substantial decrease in the bulk osmotic pressure. The osmotic pressure at the membrane surface π_{DM} was calculated using Eq. [5] and plotted as a function of bulk DS osmotic pressure in **Fig.** 9b. The modulus of $\boldsymbol{CP_D}$ was calculated from to Eq. [6] and plotted as a function of experimental water flux J_{we} (**Fig.** 9c) and function of the DS concentration (**Fig.** 9d).

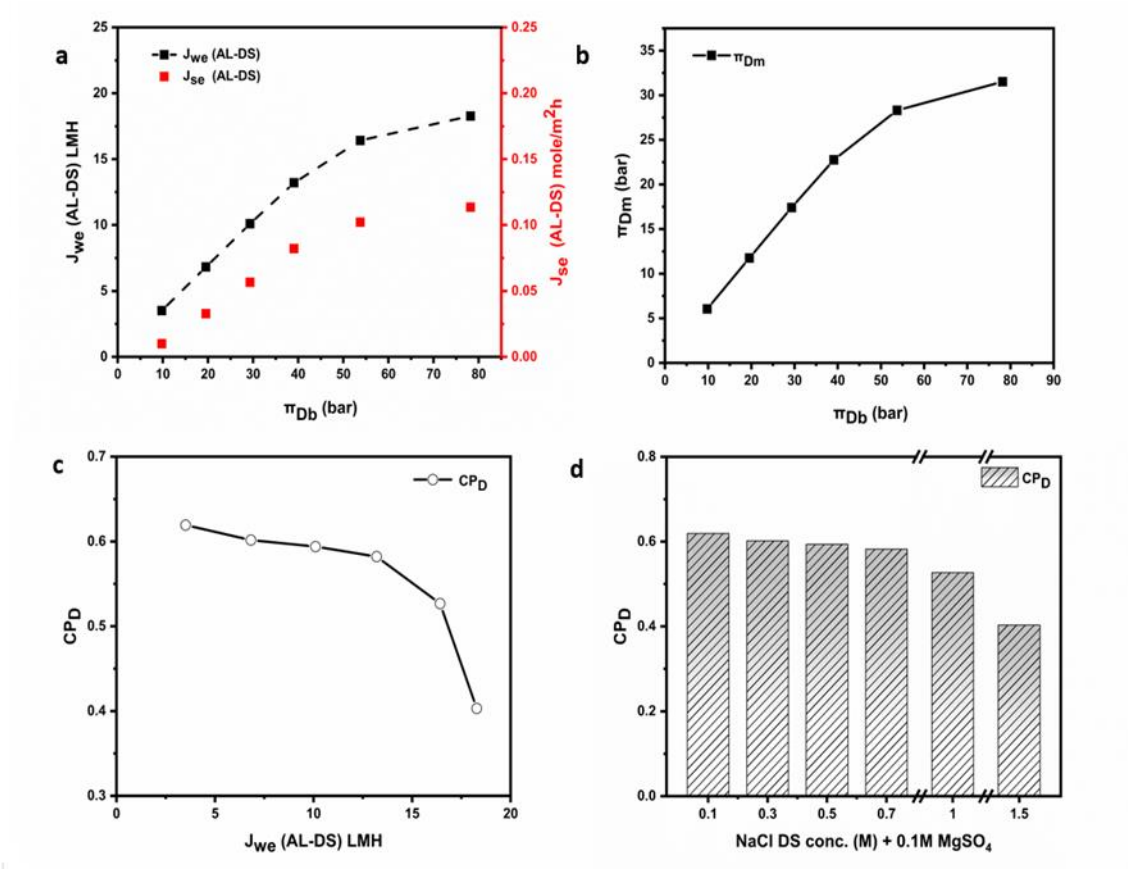

Figure 9. Quantifying dilutive concentration polarisation in the FO process for AL-DS mode with DI water feed solution, (a) Plot of experimental water flux J_{we} and RSF J_{se} against the bulk osmotic pressure, (b) Plot of osmotic pressure at the membrane surface π_{DM} against bulk osmotic pressure π_{Db} , (c) Plot of dilutive CP modulus as a function of experimental water flux, (d) CP modulus against NaCl (0.3 to 1.5M) +0.1$MgSO_4$ draw solution concentration.

The results revealed that CPD for a mixed DS was more severe compared to a single DS. This can be attributed to the fact that the concentration of divalent ions on the membrane AL (DS side) increased more abruptly (due to their lower diffusivities), leading to a higher concentration on the membrane surface [54]. Table 1 shows the value of $\boldsymbol{CP_D}$ and osmotic pressure values for NaCl and mixture DS. The osmotic pressure drop due to the dilution of DS, i.e. $\pi_{Db} - \pi_{DM}$, of a mixture DS is approximately 6 bar higher than that for NaCl draw solution.

Table 1. Osmotic pressure values and $\boldsymbol{CP_D}$ for single NaCl (1M) and mixed DS (1M+0.1M).

DS	Concentration	$\boldsymbol{\pi_{Db}}$	$\boldsymbol{\pi_{DM}}$	$\boldsymbol{\pi_{Db} - \pi_{DM}}$	$\boldsymbol{CP_D}$
NaCl	1M	48.86 bar	29.50 bar	19.36 bar	0.60
NaCl+$MgSO_4$	1M+0.1M	53.75 bar	28.31 bar	25.44 bar	0.53

4.3.2. AL-DS mode: Quantification of CP_F mixture DS-NaCl FS

To calculate the modulus of concentrative polarization, $\boldsymbol{CP_F}$, a mixture DS of 1M NaCl + 0.1M $MgSO_4$, was the DS, and NaCl in a concentration ranging from 0.05 to 0.5M was the FS. The experimental water flux J_{we} and RSF J_{se} as a function of the osmotic driving force are presented in **Fig.** 10a. The $\boldsymbol{CP_F}$ is plotted against the experimental water flux in **Fig.** 10b. The $\boldsymbol{CP_F}$ for a mixture DS ranged from 1.08 to 3.30 (Table 2). Water flux is slightly lowered in mixture DS tests leading to a relatively smaller concentration of the FS inside the SL. The RSF of the DS was also smaller in the case of mixture DS tests, which further reduced the impact of RSF on concentrative ICP. The plot of $\boldsymbol{CP_F}$ as a function of the osmotic driving force shows an exponential relationship (Fig 10b). The osmotic pressure at the membrane surface on the feed side π_{FM} was calculated from Eq. [10] and plotted against the osmotic pressure of FS (**Fig.** 10c). **Fig.** 10d shows that experimental water flux declined (almost linearly) with increasing the values of π_{FM}.

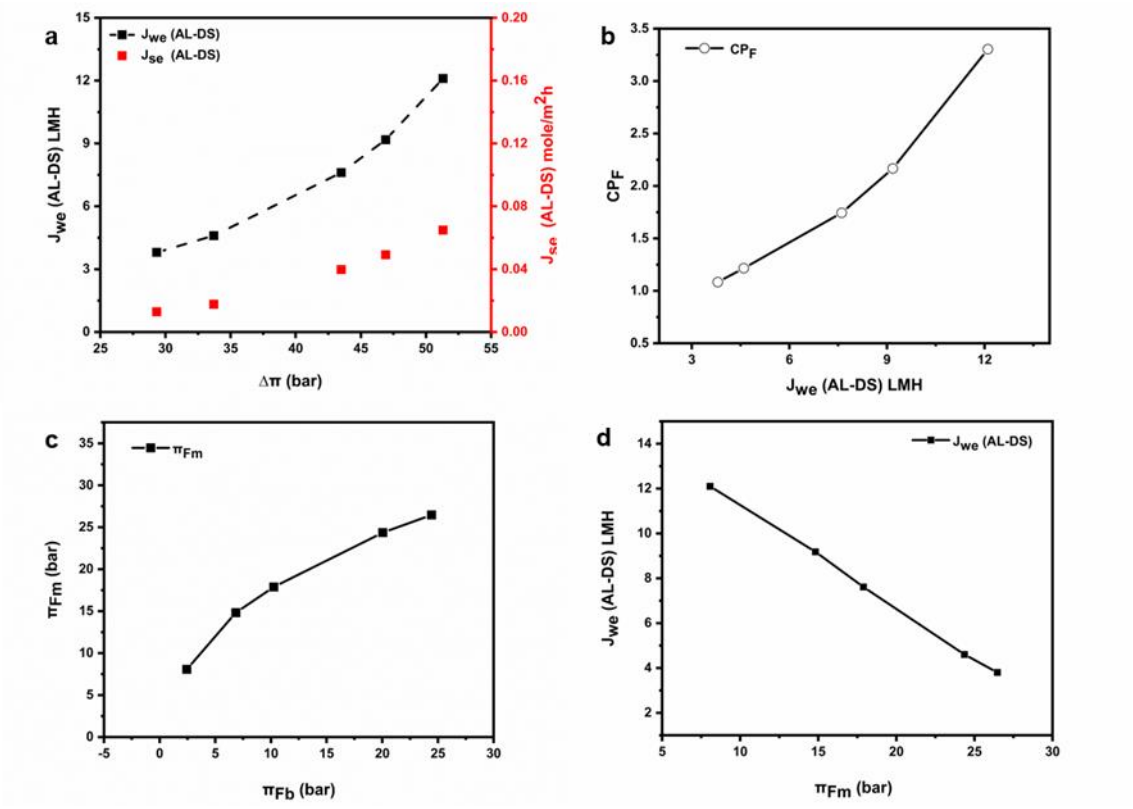

521

522 **Figure** 10. Performance of FO membrane in AL-DS mode with mixed DS, (a) Plot of
523 experimental water flux and RSF against bulk osmotic pressure, (b) Plot of concentrative CP
524 ***CP*$_F$** against experimental water flux, (c) Plot of bulk feed osmotic pressure π_{Fb} against osmotic
525 pressure at the membrane surface π_{FM}, (d). Correlation between experimental water flux and
526 osmotic pressure at the membrane surface π_{FM}.

527

528 Table 2. CP moduli for various feed solution concentration with 1M NaCl + 0.1M $MgSO_4$ DS
529 (AL-DS mode)

DS Concentration	Feed solution NaCl	***CP*$_D$** (from Fig 9c)	***CP*$_F$** (Eq.12)
1M NaCl + 0.1$MgSO_4$	0.05M	0.54	3.30
1M NaCl + 0.1$MgSO_4$	0.14M	0.57	2.17
1M NaCl + 0.1$MgSO_4$	0.21M	0.58	1.74
1M NaCl + 0.1$MgSO_4$	0.41M	0.60	1.22
1M NaCl + 0.1$MgSO_4$	0.50M	0.61	1.08

530

531 **4.3.3. AL-FS mode: Quantification of CP_D mixture DS-DI water FS**

532

533 When a mixture DS of NaCl (0.3-1.5M) + 0.1M $MgSO_4$ is placed against the SL, and DI water
534 FS is against the AL, the experimental water flux J_{we} and RSF J_{se} as a function of osmotic

driving force are presented in **Fig.** 11a. The π_{DM} value was calculated using Eq. [5] and is plotted against the osmotic pressure of DS in **Fig.** 11b. The mixture DS is diluted inside the SL, leading to a dilutive internal CP. The modulus of CP_D was calculated from Eq. [6] and is presented in **Fig.** 11c as a function of experimental flux J_{we} and as a function of DS concentration in **Fig.** 11d. As shown in Fig 11a and 11c, as the water flux increases due to the increase in the concentration of DS, the effect of CP_D becomes more substantial. Interestingly, results showed an insignificant difference in the CP_D in the FO tests with NaCl and NaCl + $MgSO_4$ DS. For instance, for 1.5M NaCl+0.1$MgSO_4$, the value of CP_D was 0.37 compared to 0.39 for NaCl DS. Overall, the CP_D values for the mixture DS was between 0.37 and 0.58 for the range of concentrations in **Fig.** 11d.

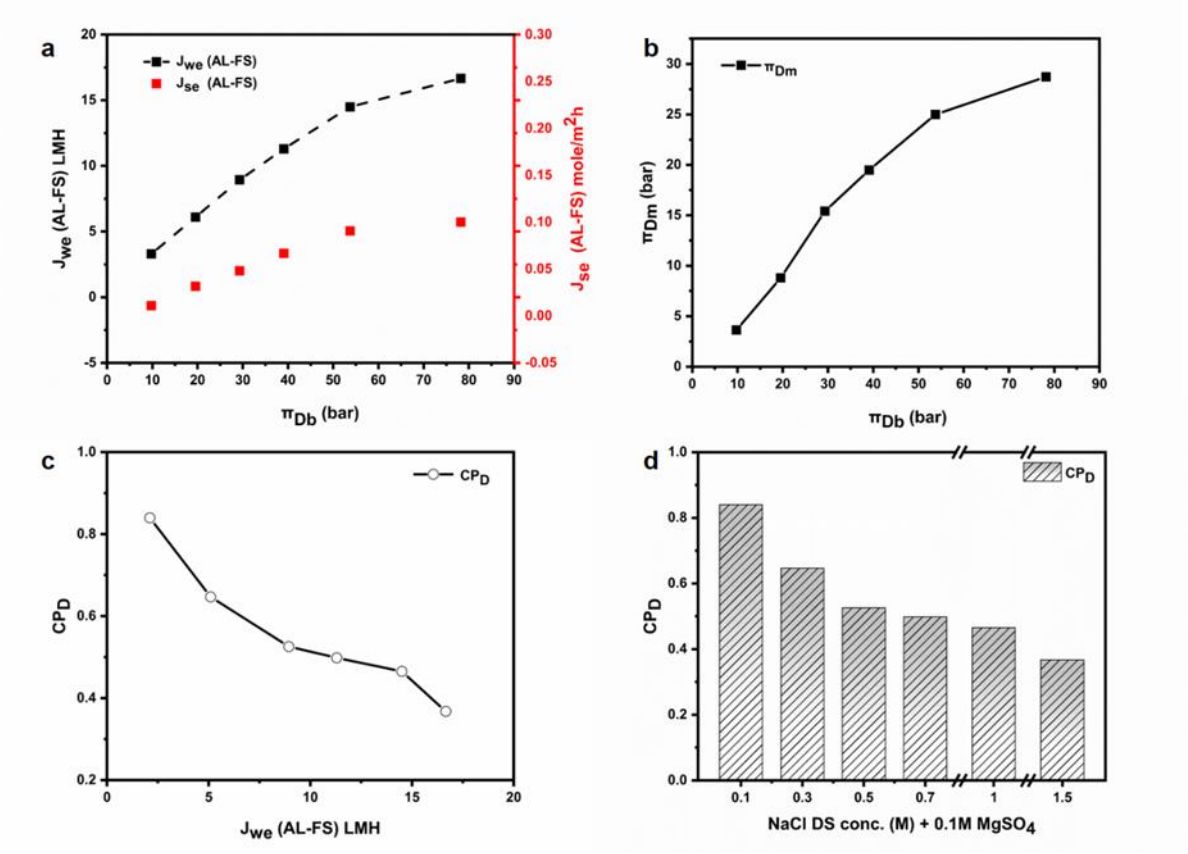

Figure 11. Quantifying dilutive concentration polarisation in the FO process for AL-FS mode with DI water feed solution, (a) Plot of experimental water flux J_{we} and RSF J_{se} against the bulk osmotic pressure (b) Plot of osmotic pressure at the membrane surface π_{DM} against bulk osmotic pressure π_{Db} (c) Plot of dilutive CP modulus as a function of experimental water flux. d). CP modulus against NaCl (0.3 to 1.5M) +0.1$MgSO_4$ draw solution concentration.

4.3.4. AL-FS mode: Quantification CP_F mixture DS-DI water FS

When the FS was replaced with NaCl 0.05M to 0.5M in the AL-FS mode, and a mixture DS was against the SL, the concentrative external CP, ***CP$_F$***, develops on the AL side of the membrane and dilutive internal CP, ***CP$_D$***, on the DS side. Water flux, J_{we}, and RSF, J_{se}, were plotted as a function of the osmotic driving force (**Fig.** 12a). The lowest RSF amongst all the experiments is achieved in the AL-FS mode with a mixture DS. The moduli of ***CP$_D$*** and ***CP$_F$*** are presented in Table 3. The ***CP$_F$*** values ranged from 1.18 to 3.27 for the FS concentration of 0.05 to 0.5M. The plot of ***CP$_F$*** as a function of experimental water flux J_{we} is Presented in **Fig.** 12b. ***CP$_F$*** can also be predicted at from the slope of the plot between the π_{FM} and π_{Fb} in **Fig.** 12c. The value of π_{FM} can also be predicted from **Fig.**12c for any feed solution osmotic pressure. Furthermore, the value of theoretical water flux in the FO process for any FS within the range of FS and DS concentrations can be predicted from **Fig.** 12d for the same range of draw solutions.

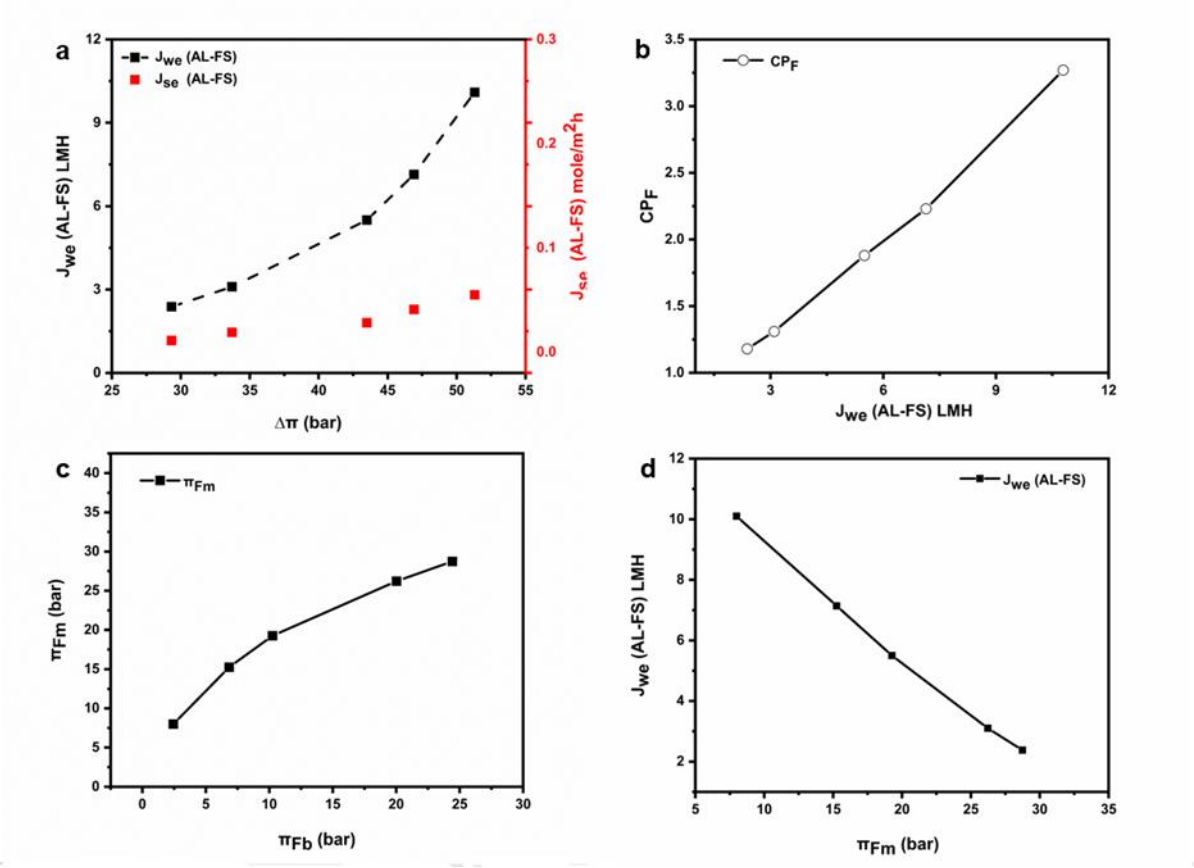

Figure 12. Performance of FO membrane in AL-FS mode with mixture DS and 0.05 to 0.5M NaCl FS, (a) Plot of experimental water flux and RSF against bulk osmotic pressure, (b) Plot of concentrative CP against experimental water flux, (c) Plot of bulk feed osmotic pressure π_{Fb} against osmotic pressure at the membrane surface π_{FM}, (d). Correlation between experimental water flux and osmotic pressure at the membrane surface.

Table 3. Moduli of dilutive and concentrative CP for various feed solution concentration with 1M NaCl + 0.1M $MgSO_4$ DS (AL-FS mode)

DS Concentration	Feed solution NaCl	CP_D (from Fig 11c)	CP_F (Eq.12)
1M NaCl + 0.1$MgSO_4$	0.05M	0.47	3.27
1M NaCl + 0.1$MgSO_4$	0.14M	0.51	2.23
1M NaCl + 0.1$MgSO_4$	0.21M	0.53	1.88
1M NaCl + 0.1$MgSO_4$	0.41M	0.59	1.31
1M NaCl + 0.1$MgSO_4$	0.50M	0.61	1.18

Table 3 shows that the CP_D values in the AL-FS mode are more severe than the CP_D in the AL-DS mode (Table 2). This is mainly because the CP_D in the AL-FS occurs inside the SL and cannot be mitigated by the high cross-flow velocities in this study.

4.4. Prediction of water flux, CP and RSF

It is possible to estimate theoretical water flux J_{wt} in the FO process with a DI water FS and NaCl DS (concentrations 0.1M-1.5M in this study), using the empirical data from the FO experiments. First, π_{Db} can be calculated to predict π_{DM} from the correlation between the two (Fig 5c and 7c for NaCl DS in AL-DS and AL-FS respectively and 9c and 11c for mixed DS in AL-DS and AL-FS respectively), then J_{wt} will be obtained from Eq. [4] using the predicted π_{DM} value. To do this, several draw solution concentrations between 0.1M and 1.5M (0.4, 0.6, 0.8, 1, 1.2, 1.3, and 1.4M) were considered for water flux prediction in the FO process using a DI water feed solution. For each DS concentration, π_{Db} was calculated to obtain π_{DM} and substituted in Eq. [4] to obtain J_{wt}. Experimental water flux was also determined for all draw solutions (0.4, 0.5, 0.6, 0.8, 1.2, and 1.4M NaCl DS for single DS and 0.1M $MgsO_4$ was added to each for mixed DS) and compared with the J_{wt} for both NaCl and mixture DS in the AL-DS and the AL-FS modes (**Fig.** 13a and **Fig.**13b). The results show an excellent agreement between J_{wt} and J_{we} for all draw solution concentrations and with an error of less than 5%. The CP_D for the investigated draw solutions can be predicted from Eq. [6] (Table A.1.5, Appendix A.1).

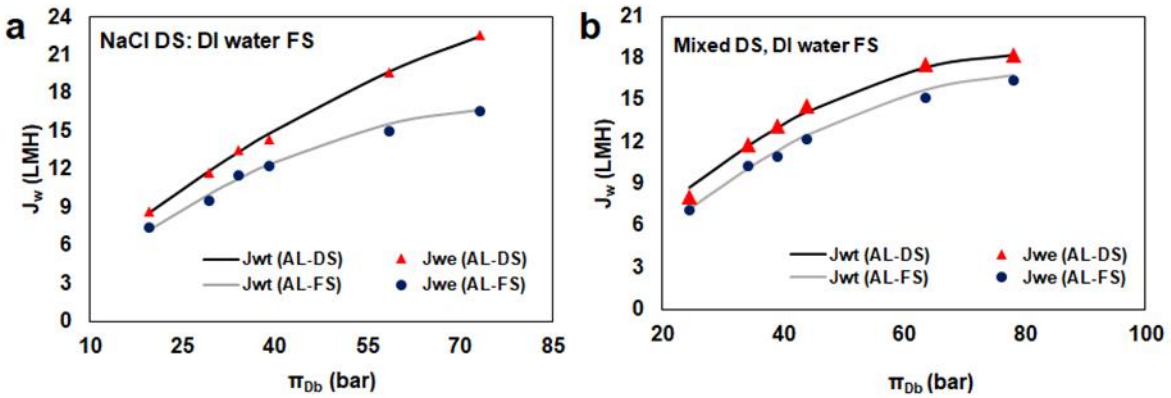

600

601 Figure 13. Theoretical flux prediction based on the correlations between empirical data, (12a)
602 0.4M to 1.4M NaCl DS and DI water FS in AL-DS and AL-FS mode, and (12b) Mixed DS with
603 DI water feed in the AL-DS and AL-FS mode.

604

605 The excellent agreement between theoretical and experimental water flux J_{we} and J_{wt} shows
606 the reliability of the proposed model to predict water flux in the FO process using empirical
607 data. Compared to the previous models, water flux in the FO membrane can be determined
608 with less information about the membrane and flow characteristics in the FO process.
609 However, feed solution in the FO process is often saline water, which leads to internal
610 concentration polarization. This issue will be covered in the following section of the study.

611 For the FO process with a saline feed solution, additional information about the correlation
612 between π_{FM} and J_{we} should be available to predict the J_{wt} and CP_F in the FO process with a
613 saline FS. Initially π_{Fb} and π_{Db} were calculated as an average of the inlet and the outlet
614 concentration of the feed and draw solutions. DS used was 1M NaCl DS experiments and
615 1M+0.1M $MgSO_4$ in mixed DS experiments. For each FS concentration, the osmotic
616 pressure π_{Fb} was determined as the average inlet and outlet FS osmotic pressure and then
617 the value of π_{FM} was obtained from the correlations in **Fig.**6c, **Fig.**8c, **Fig.**10c and **Fig.**12c.
618 The value of J_{wt} was then predicted for NaCl and mixture DS using the correlations between
619 J_{we} and π_{FM} as shown in **Fig**. 14a and **Fig.** 14b, respectively. The percentage error ranged
620 from 4% to 5% for the experimental and theoretical values. The values of π_{FM} and J_{wt} was
621 compensated in Eq. [8a] to obtain the value of π_{DM}. Furthermore, CP_F can be predicted from
622 Eq. [10] and CP_D from Eq. [6], since all the input values in these equations are in Appendix
623 A.1 (Table A.1.6).

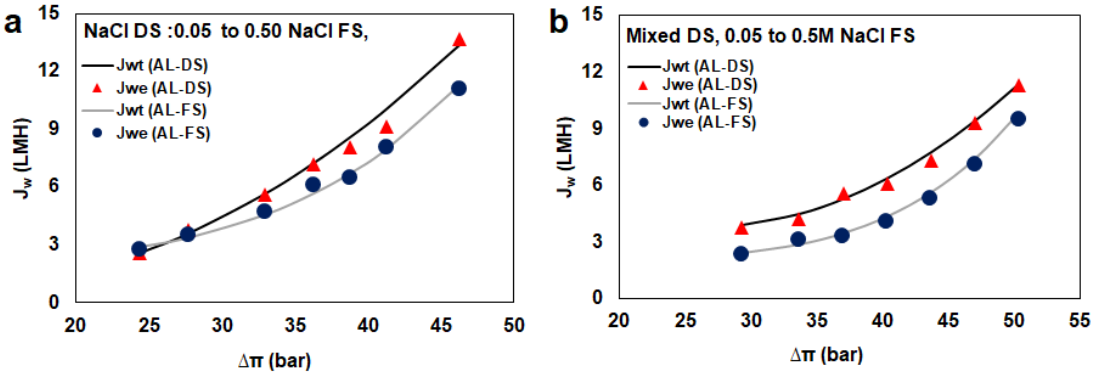

Figure 14. Prediction of theoretical water flux with NaCl feed solution (3g/L to 29.5g/L) in the AL-FS and the AL-DS mode, (a) Plot of theoretical and experimental water flux as a function of the osmotic driving force for single NaCl DS 1M and FS of 3g/L, 9g/L, 12g/L, 15g/L,19g/L,25.20g/L and 29.20g/L NaCl solution in the AL-FS and the AL-DS mode (b) Plot of theoretical and experimental water flux with 1M NaCl+0.1M $MgSO_4$ DS and FS of 4g/L, 8g/L,12g/L,16g/L, 20g/L, 24g/L and 29.20g/L NaCl in the AL-FS and the AL-DS mode. All prediction was based on empirical data.

From **Fig.**14a and 14b, the proposed model can provide a good estimation of theoretical water flux for any FS within the range of experimental data. For instance, J_{wt}, CP_F, **and** CP_D of any NaCl FS from 0.05 M-0.5M can be estimated using the methodology in this study. Apart from predicting the parameters above, the theoretical RSF J_{st} in the FO process can also be predicted, since the value of solute concentrations at the membrane surface C_{Dm} and C_{Fm} can be determined easily once the value of π_{DM} and π_{FM} is available. The theoretical RSF can then be predicted from Eq.[8]. The experimental RSF was determined from Eq. [10]. The theoretical and experimental RSF are compared in **Fig.**15a &15b for NaCl and a mixture DS, respectively; results showed less than 10% error between the theoretical and experimental values. As evident from **Fig.**15a and **Fig.** 15b, the model can provide a good estimation of the RSF based on the solute concentration profiles at the membrane surface. The error was slightly larger in the RSF prediction for mixed DS compared to the single NaCl DS.

The proposed empirical model can provide solute concentration profiles of the FO membrane and quantify CP in the FO process. Most importantly, this model does not rely on hydrodynamic relations such as Reynold and Sherwood relations and the solute resistance to diffusion “K” value.

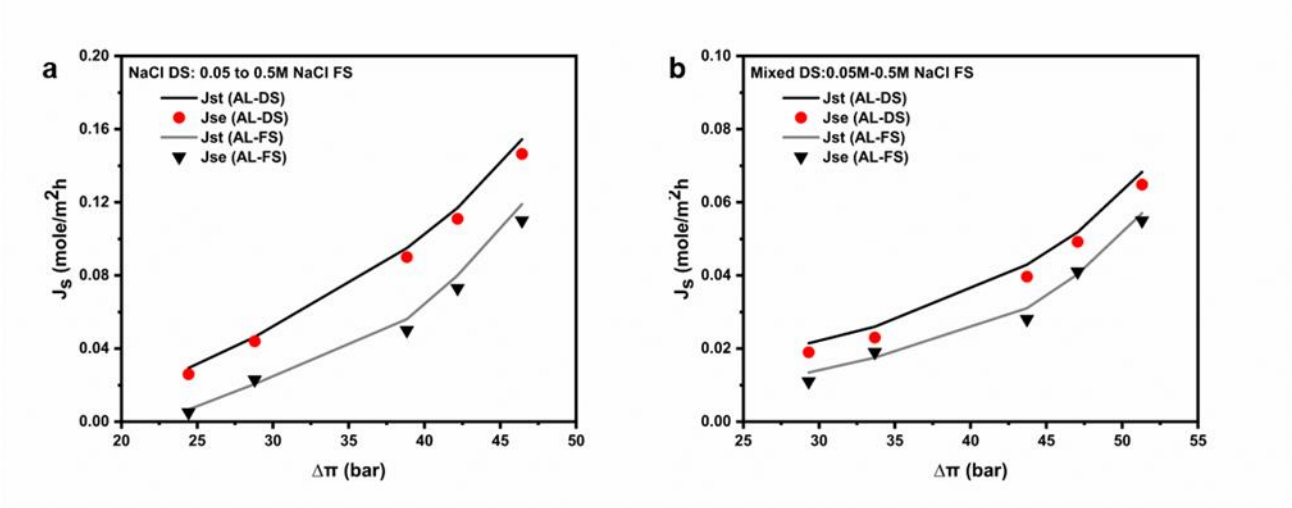

651

652 **Figure 15**. Comparison of theoretical RSF J_{st} and experimental RSF J_{se} , (a) For 1M NaCl DS
653 and 0.05 to 0.5M NaCl FS, (b) For 1M NaCl+0.1M $MgSO_4$ DS and 0.05M to 0.5M NaCl FS.

654

655 **5. Conclusion**

656

657 The moduli of CPs' in the FO process require a large amount of information to calculate. The
658 existing models can predict the experimental flux in the FO process. Still, they become more
659 demanding when a mixture of draw solutions is used or lack of information about the FO
660 modules due to propriety issues. Therefore, the solute resistivity "*K*" and mass transfer
661 coefficient "*k*" value are hard to determine for a forward osmosis system. The empirical model
662 in this study can provide an alternative solution for the prediction of water flux in the FO
663 process. The model demonstrated an excellent capability to predict CP and water flux in the
664 FO process with 95-99% agreement with experimental values and without the need to obtain
665 experimental parameters such as *K* and *k*. The model can be particularly helpful in the FO
666 processes using a mixture of draw solutions. In a multicomponent draw solution, the diffusion
667 coefficient is hardly available in the literature and ions to move at a distinct rate within the film
668 layer; therefore, it is impossible to define an effective diffusivity of the mixture. The model in
669 this study only relies on a set of experimental data to measure CP and predict performance,
670 such as Flux, CP, and RSF. It can also be extended to ternary and quaternary mixtures of
671 DSs as well as commercial spiral wound modules.

672

Acknowledgements

This research is made possible by NPRP award (NPRP10-0117-170176) from Qatar National Research Fund (QNRF). This work is also supported by an Australian government research training program scholarship provided to Ibrar Ibrar.

Appendix A.1

A.1.1

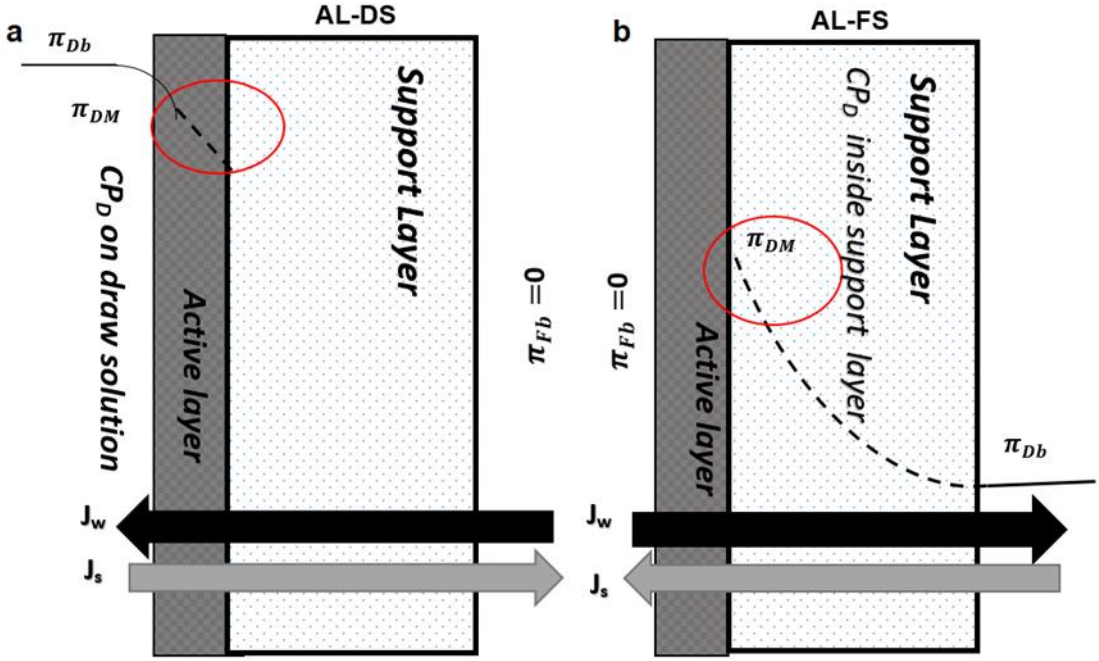

Figure.A.1. An illustration of concentration profiles in the AL-DS and the AL-FS mode with DI water FS, (a) The AL (active layer) of the membrane facing the draw solution and the support layer faces the feed solution in the AL-DS mode. The bulk osmotic pressure difference is equal to the difference between membrane surface osmotic pressures, (b) The AL of the membrane is facing the feed solution, and the support layer is facing the draw solution in the AL-FS mode. It should be noted that the membrane is assumed to have a 100% rejection of ions.

A.1.2. Pure water permeability, salt permeability of FO membrane

A reverse osmosis (RO) test was performed to determine membrane water and salt permeability coefficients, A_w and B, respectively. RO test was performed with DI water feed solution at 20°C and feed pressure increased from 1 to 6 bar with 0.5 bar increment to determine the value of A_w. The AL of the FO membrane was facing DI water to avoid membrane deformity. First, the membrane was compacted with maximum hydraulic pressure

of three bar until the permeate flux reached a steady state. A concentrate/back pressure control valve was used to adjust trans-membrane pressure. Following the membrane compaction, the next reading was collected after 12 hours using the same hydraulic pressure. The water flux was calculated according to Eq. [13], and the value of A_w was calculated using Eq. [1].

$$A_w = \frac{J_w}{\Delta P} \qquad [1]$$

The value of A_w was 0.58 $Lm^{-2}h^{-1}bar^{-1}$. The membrane rejection rate was carried out using 2 g/L NaCl feed solution at 20°C. The test was carried out at 6 bar, and B value was calculated from the following expression:

$$B = \frac{(1-R_j)}{R_j} J_w \qquad [2]$$

where R_j is the rejection rate of the membrane. The B value in this study was 0.32±0.07 L/m^2h for NaCl feed solution. The values of A_w and B are comparable to the values previously reported for this FO membrane [35].

A.1.3. CP for 1M NaCl DS and 0.05M to 0.50M FS (AL-DS mode)

The modulus of ***CP_D*** was predicted from Fig.6c, and the ***CP_F*** was then calculated from Eq. [9] listed in Table A.1.

Table A.1.3 CP moduli for various feed solution concentration with 1M NaCl DS (AL-DS mode)

DS (NaCl)	Feed solution	CP_D (Predicted from Fig 5c)	CP_F (Eq.12)
1M	0.05M	0.67	3.72
1M	0.14M	0.75	2.79
1M	0.21M	0.80	2.45
1M	0.41M	0.93	1.91
1M	0.50M	0.98	1.78

A.1.4. CP for 1M NaCl DS and 0.05M to 0.50M FS (AL-FS mode)

721 The CP_D was predicted from Fig.8c, and the CP_F was then calculated from Eq. [9] listed in
722 Table A.2.

723

724 Table A.1.4. CP moduli for 0.05M to 0.5M NaCl feed solution and1M NaCl DS (AL-FS mode)

DS Concentration	Feed solution NaCl	CP_D (predicted from Fig 7c)	CP_F (Eq.12)
1M	0.05M	0.56	3.06
1M	0.14M	0.59	2.18
1M	0.21M	0.62	1.89
1M	0.41M	0.69	1.36
1M	0.50M	0.74	1.28

725

726 **A.1.5. CP_D for various DS concentration with DI water FS (AL-DS mode and AL-FS**
727 **mode)**
728

729 Table A.1.5. CP moduli data for single and mixed DS with DI water feed solution.

DS Concentration	Feed solution	CP_D (predicted) AL-DS	CP_D (predicted) AL-FS
0.4 NaCl	DI water	0.76	0.64
0.6 NaCl	DI water	0.70	0.59
0.8 NaCl	DI water	0.68	0.57
1.2 NaCl	DI water	0.66	0.55
1.4 NaCl	DI water	0.58	0.46
0.4NaCl+0.1$MgSO_4$	DI water	0.62	0.52
0.6 NaCl+0.1$MgSO_4$	DI water	0.59	0.51
0.8 NaCl+0.1$MgSO_4$	DI water	0.58	0.50
1.2 NaCl+0.1$MgSO_4$	DI water	0.56	0.49
1.4 NaCl+0.1$MgSO_4$	DI water	0.47	0.43

730

731 **A.1.6. CP_D and CP_F for 1M DS and NaCl FS (AL-DS mode and AL-FS mode)**
732

733 Table A.1.6. CP moduli data for single and mixed DS with NaCl feed solution (0.05 to 0.5M)

DS Concentration	FS NaCl (M)	CP_D (predicted) AL-DS	CP_F (predicted) AL-DS	CP_D (predicted) AL-FS	CP_F (predicted) AL-FS
1M NaCl	0.05	0.67	3.79	0.56	3.17
1M NaCl	0.15	0.76	2.64	0.60	2.04
1M NaCl	0.21	0.80	2.44	0.62	1.85

1M NaCl	0.26	0.84	2.29	0.64	1.71
1M NaCl	0.33	0.89	2.12	0.67	1.56
1M NaCl	0.43	0.95	1.90	0.71	1.37
1M NaCl	0.50	0.98	1.77	0.73	1.26
1M NaCl+0.1$MgSO_4$	0.05	0.55	2.90	0.50	2.94
1M NaCl+0.1$MgSO_4$	0.15	0.56	2.10	0.55	2.54
1M NaCl+0.1$MgSO_4$	0.21	0.58	1.77	0.61	2.32
1M NaCl+0.1$MgSO_4$	0.26	0.59	1.55	0.67	2.14
1M NaCl+0.1$MgSO_4$	0.33	0.60	1.38	0.72	1.97
1M NaCl+0.1$MgSO_4$	0.43	0.61	1.24	0.77	1.81
1M NaCl+0.1$MgSO_4$	0.50	0.62	1.07	0.81	1.62

References

[1] A. Achilli, T.Y. Cath, A.E. Childress, Power generation with pressure retarded osmosis: An experimental and theoretical investigation, Journal of Membrane Science, 343 (2009) 42-52.

[2] B.S. Chanukya, S. Patil, N.K. Rastogi, Influence of concentration polarization on flux behavior in forward osmosis during desalination using ammonium bicarbonate, Desalination, 312 (2013) 39-44.

[3] J.R. McCutcheon, R.L. McGinnis, M. Elimelech, Desalination by ammonia–carbon dioxide forward osmosis: Influence of draw and feed solution concentrations on process performance, Journal of Membrane Science, 278 (2006) 114-123.

[4] N.C. Nguyen, S.S. Chen, S. Jain, H.T. Nguyen, S.S. Ray, H.H. Ngo, W. Guo, N.T. Lam, H.C. Duong, Exploration of an innovative draw solution for a forward osmosis-membrane distillation desalination process, Environ Sci Pollut Res Int, 25 (2018) 5203-5211.

[5] A.P. Straub, A. Deshmukh, M. Elimelech, Pressure-retarded osmosis for power generation from salinity gradients: is it viable?, Energy & Environmental Science, 9 (2016) 31-48.

[6] Y.-N. Wang, K. Goh, X. Li, L. Setiawan, R. Wang, Membranes and processes for forward osmosis-based desalination: Recent advances and future prospects, Desalination, 434 (2018) 81-99.

[7] H. Zhang, S. Cheng, F. Yang, Use of a spacer to mitigate concentration polarization during forward osmosis process, Desalination, 347 (2014) 112-119.

[8] A. Altaee, J. Zhou, A.A. Alanezi, G. Zaragoza, Pressure retarded osmosis process for power generation: Feasibility, energy balance and controlling parameters, Applied Energy, 206 (2017) 303-311.

[9] J. Heikkinen, H. Kyllönen, E. Järvelä, A. Grönroos, C.Y. Tang, Ultrasound-assisted forward osmosis for mitigating internal concentration polarization, Journal of Membrane Science, 528 (2017) 147-154.

763 [10] E.M.V. Hoek, M. Elimelech, Cake-Enhanced Concentration Polarization: A New Fouling
764 Mechanism for Salt-Rejecting Membranes, Environmental Science & Technology, 37 (2003)
765 5581-5588.
766 [11] J.R. McCutcheon, M. Elimelech, Influence of concentrative and dilutive internal
767 concentration polarization on flux behavior in forward osmosis, Journal of Membrane
768 Science, 284 (2006) 237-247.
769 [12] C.H. Tan, H.Y. Ng, Modified models to predict flux behavior in forward osmosis in
770 consideration of external and internal concentration polarizations, Journal of Membrane
771 Science, 324 (2008) 209-219.
772 [13] C.D. Moody, J.O. Kessler, Forward osmosis extractors, Desalination, 18 (1976) 283-295.
773 [14] N.-N. Bui, J.T. Arena, J.R. McCutcheon, Proper accounting of mass transfer resistances in
774 forward osmosis: Improving the accuracy of model predictions of structural parameter,
775 Journal of Membrane Science, 492 (2015) 289-302.
776 [15] D. Emadzadeh, W.J. Lau, T. Matsuura, M. Rahbari-Sisakht, A.F. Ismail, A novel thin film
777 composite forward osmosis membrane prepared from PSf–TiO2 nanocomposite substrate
778 for water desalination, Chemical Engineering Journal, 237 (2014) 70-80.
779 [16] B. Khorshidi, A. Bhinder, T. Thundat, D. Pernitsky, M. Sadrzadeh, Developing high
780 throughput thin film composite polyamide membranes for forward osmosis treatment of
781 SAGD produced water, Journal of Membrane Science, 511 (2016) 29-39.
782 [17] J.R. Mccutcheon, M. Elimelech, Modeling water flux in forward osmosis: Implications
783 for improved membrane design, AIChE Journal, 53 (2007) 1736-1744.
784 [18] C.H. Tan, H.Y. Ng, Revised external and internal concentration polarization models to
785 improve flux prediction in forward osmosis process, Desalination, 309 (2013) 125-140.
786 [19] C.Y. Tang, Q. She, W.C.L. Lay, R. Wang, A.G. Fane, Coupled effects of internal
787 concentration polarization and fouling on flux behavior of forward osmosis membranes
788 during humic acid filtration, Journal of Membrane Science, 354 (2010) 123-133.
789 [20] K.Y. Wang, R.C. Ong, T.-S. Chung, Double-Skinned Forward Osmosis Membranes for
790 Reducing Internal Concentration Polarization within the Porous Sublayer, Industrial &
791 Engineering Chemistry Research, 49 (2010) 4824-4831.
792 [21] I. Ibrar, A. Altaee, J.L. Zhou, O. Naji, D. Khanafer, Challenges and potentials of forward
793 osmosis process in the treatment of wastewater, Critical Reviews in Environmental Science
794 and Technology, (2019) 1-45.
795 [22] I. Ibrar, S. Yadav, A. Altaee, A.K. Samal, J.L. Zhou, T.V. Nguyen, N. Ganbat, Treatment of
796 biologically treated landfill leachate with forward osmosis: Investigating membrane
797 performance and cleaning protocols, Science of The Total Environment, 744 (2020) 140901.
798 [23] Y. Wang, M. Zhang, Y. Liu, Q. Xiao, S. Xu, Quantitative evaluation of concentration
799 polarization under different operating conditions for forward osmosis process, Desalination,
800 398 (2016) 106-113.
801 [24] M.F. Gruber, C.J. Johnson, C.Y. Tang, M.H. Jensen, L. Yde, C. Hélix-Nielsen,
802 Computational fluid dynamics simulations of flow and concentration polarization in forward
803 osmosis membrane systems, Journal of Membrane Science, 379 (2011) 488-495.
804 [25] I. Ibrar, O. Naji, A. Sharif, A. Malekizadeh, A. Alhawari, A.A. Alanezi, A. Altaee, A Review
805 of Fouling Mechanisms, Control Strategies and Real-Time Fouling Monitoring Techniques in
806 Forward Osmosis, Water, 11 (2019) 695.
807 [26] A. Altaee, A. Sharif, G. Zaragoza, N. Hilal, Dual stage PRO process for power generation
808 from different feed resources, Desalination, 352 (2014) 118-127.

809 [27] S. Yadav, H. Saleem, I. Ibrar, O. Naji, A.A. Hawari, A.A. Alanezi, S.J. Zaidi, A. Altaee, J.
810 Zhou, Recent developments in forward osmosis membranes using carbon-based
811 nanomaterials, Desalination, 482 (2020) 114375.
812 [28] S. Yadav, I. Ibrar, A. Altaee, A.K. Samal, R. Ghobadi, J. Zhou, Feasibility of brackish water
813 and landfill leachate treatment by GO/MoS2-PVA composite membranes, Science of The
814 Total Environment, 745 (2020) 141088.
815 [29] I. Sutzkover, D. Hasson, R. Semiat, Simple technique for measuring the concentration
816 polarization level in a reverse osmosis system, Desalination, 131 (2000) 117-127.
817 [30] I. Sutzkover, D. Hasson, R. Semiat, Simple technique for measuring the concentration
818 polarization level in a reverse osmosis system, Desalination, 131 (2000) 117-127.
819 [31] S. Lee, C.-H. Lee, Effect of operating conditions on CaSO4 scale formation mechanism in
820 nanofiltration for water softening, Water Research, 34 (2000) 3854-3866.
821 [32] E. Matthiasson, B. Sivik, Concentration polarization and fouling, Desalination, 35 (1980)
822 59-103.
823 [33] A. Abdelrasoul, H. Doan, A. Lohi, C.-H. Cheng, Mass transfer mechanisms and transport
824 resistances in membrane separation process, in: Mass Transfer-Advancement In Process
825 Modelling, IntechOpen, 2015.
826 [34] R.E. Treybal, Mass transfer operations, New York, 466 (1980).
827 [35] H.T. Madsen, S.S. Nissen, J. Muff, E.G. Søgaard, Pressure retarded osmosis from
828 hypersaline solutions: investigating commercial FO membranes at high pressures,
829 Desalination, 420 (2017) 183-190.
830 [36] R.W. Holloway, R. Maltos, J. Vanneste, T.Y. Cath, Mixed draw solutions for improved
831 forward osmosis performance, Journal of Membrane Science, 491 (2015) 121-131.
832 [37] S. Phuntsho, H.K. Shon, T. Majeed, I. El Saliby, S. Vigneswaran, J. Kandasamy, S. Hong, S.
833 Lee, Blended Fertilizers as Draw Solutions for Fertilizer-Drawn Forward Osmosis
834 Desalination, Environmental Science & Technology, 46 (2012) 4567-4575.
835 [38] P. Liu, B. Gao, H.K. Shon, D. Ma, H. Rong, P. Zhao, S. Zhao, Q. Yue, Q. Li, Water flux
836 behavior of blended solutions of ammonium bicarbonate mixed with eight salts respectively
837 as draw solutions in forward osmosis, Desalination, 353 (2014) 39-47.
838 [39] J.Y. Law, A.W. Mohammad, Multiple-solute salts as draw solution for osmotic
839 concentration of succinate feed by forward osmosis, Journal of Industrial and Engineering
840 Chemistry, 51 (2017) 264-270.
841 [40] O. Medvedev, A. Shapiro, Diffusion coefficients in multicomponent mixtures, (2005).
842 [41] J. Jawad, A.H. Hawari, S. Zaidi, Modeling of forward osmosis process using artificial
843 neural networks (ANN) to predict the permeate flux, Desalination, 484 (2020) 114427.
844 [42] Q. Wang, Z. Zhou, J. Li, Q. Tang, Y. Hu, Modeling and measurement of temperature and
845 draw solution concentration induced water flux increment efficiencies in the forward
846 osmosis membrane process, Desalination, 452 (2019) 75-86.
847 [43] J. Lee, N. Ghaffour, Predicting the performance of large-scale forward osmosis module
848 using spatial variation model: Effect of operating parameters including temperature,
849 Desalination, 469 (2019) 114095.
850 [44] N.C. Nguyen, H.C. Duong, H.T. Nguyen, S.-S. Chen, H.Q. Le, H.H. Ngo, W. Guo, C.C.
851 Duong, N.C. Le, X.T. Bui, Forward osmosis–membrane distillation hybrid system for
852 desalination using mixed trivalent draw solution, Journal of Membrane Science, 603 (2020)
853 118029.
854 [45] M. Hamdan, A.O. Sharif, G. Derwish, S. Al-Aibi, A. Altaee, Draw solutions for Forward
855 Osmosis process: Osmotic pressure of binary and ternary aqueous solutions of magnesium

chloride, sodium chloride, sucrose and maltose, Journal of Food Engineering, 155 (2015) 10-15.
[46] W.A. Phillip, J.S. Yong, M. Elimelech, Reverse Draw Solute Permeation in Forward Osmosis: Modeling and Experiments, Environmental Science & Technology, 44 (2010) 5170-5176.
[47] A. Altaee, J. Zhou, A. Alhathal Alanezi, G. Zaragoza, Pressure retarded osmosis process for power generation: Feasibility, energy balance and controlling parameters, Applied Energy, 206 (2017) 303-311.
[48] N.Y. Yip, M. Elimelech, Performance limiting effects in power generation from salinity gradients by pressure retarded osmosis, Environmental science & technology, 45 (2011) 10273-10282.
[49] J.R. McCutcheon, M. Elimelech, Influence of concentrative and dilutive internal concentration polarization on flux behavior in forward osmosis, Journal of Membrane Science, 284 (2006) 237-247.
[50] B. Hribar, N.T. Southall, V. Vlachy, K.A. Dill, How ions affect the structure of water, Journal of the American Chemical Society, 124 (2002) 12302-12311.
[51] K.D. Collins, Charge density-dependent strength of hydration and biological structure, Biophysical journal, 72 (1997) 65-76.
[52] R.E. Kesting, Semipermeable membranes of cellulose acetate for desalination in the process of reverse osmosis. I. Lyotropic swelling of secondary cellulose acetate, Journal of Applied Polymer Science, 9 (1965) 663-688.
[53] M.C.Y. Wong, K. Martinez, G.Z. Ramon, E.M.V. Hoek, Impacts of operating conditions and solution chemistry on osmotic membrane structure and performance, Desalination, 287 (2012) 340-349.
[54] S. Déon, P. Dutournié, P. Fievet, L. Limousy, P. Bourseau, Concentration polarization phenomenon during the nanofiltration of multi-ionic solutions: Influence of the filtrated solution and operating conditions, Water Research, 47 (2013) 2260-2272.